AIMS Mathematics, 11(6): 17492–17527.
DOI: 10.3934/math.2026715
Received: 17 April 2026
Revised: 23 May 2026
Accepted: 05 June 2026
Published: 16 June 2026

https://www.aimspress.com/journal/Math

Research article

Non-perturbative analysis of bifurcation and chaotic dynamics of a cantilever beam under triple time-delayed feedback control

Ahmad Almutlg[1], Galal M. Moatimid[2], T. S. Amer[3] and Yasmeen M. Mohamed[2,*]

[1] Department of Mathematics, College of Science, Qassim University, P.O. Box 6644, Buraydah 51452, Saudi Arabia
[2] Department of Mathematics, Faculty of Education, Ain Shams University, Roxy, Cairo, 11566, Egypt
[3] Department of Mathematics, Faculty of Science, Tanta University, Tanta 31527, Egypt

* **Correspondence:** Email: yasmeenmostafa@edu.asu.edu.eg.

Abstract: In this work, we aimed to improve vibration suppression in a flexible CB structure through the application of time-delays nonlinear feedback control, surpassing conventional linear control under external excitation. To improve the effectiveness and stability of vibration lessening in flexible constructions exposed to external perturbations, three time-delayed nonlinear feedback controllers provided enhanced attenuation of the fundamental CB responses compared to conventional linear or instantaneous control. The controllers employed linear/nonlinear procedures of position, velocity, and acceleration. The core methodology was based on the non-perturbative approach, mainly derived from He's frequency formula, which converted a weakly nonlinear oscillator of an ordinary differential equation into an equivalent linear one. The resulting parametric ODE was validated using the Mathematica Software. The stability/instability analyses were explored under multiple scenarios. Moreover, two objective functions were developed to optimize control gains and delay parameters for effective vibration suppression and bifurcation control. Furthermore, the method was grounded in first principles, diminished analytical complexity, and maintained high numerical accuracy in treating nonlinear parametric systems. To explore the nonlinear dynamics of the CB, several tools were employed, including bifurcation diagrams, Poincaré sections, phase portraits, and the largest Lyapunov exponents.

Keywords: cantilever beam; nonlinear dynamics; time-delayed feedback control; non-perturbative approach; He's frequency formula; bifurcation analysis; Poincaré sections; largest Lyapunov

exponent; chaotic transitions; stability maps; nonlinear systems; differential equations
Mathematics Subject Classification: 37N35, 70K42, 74K10, 37D45, 37G35, 93D15

Abbreviations

Symbol	Meaning	Symbol	Meaning
CB	Cantilever beam	LEE	Largest Lyapunov exponents
NPA	Non-perturbative approach	PM	Poincaré map
HFF	He's frequency formula	MEMS	Micro-electromechanical systems
ODE	Ordinary differential equation	MFC	Macro-fiber composite
MS	Mathematica Software	DO	Duffing oscillator
NS	Numerical solution	BD	Bifurcation diagram
IC	Initial condition	MTSM	Multiple time-scales method
		HBM	Harmonic balance method

1. Introduction

The CB is one of the most fundamental structural elements in engineering due to its simple configuration, adaptability, and wide range of applications. Fixed at one end and free at the other, it serves as an essential model for engineering systems such as bridges, aircraft wings, turbine blades, MEMS devices, and biological structures. Its significance lies in its ability to sustain bending, shear, and vibrational loads while providing key insights into resonance, stability, and structural failure mechanisms. Consequently, the CB has become a benchmark system in theoretical and applied mechanics. The nonlinear response of slender CBs subjected to parametric excitation has attracted considerable attention in the literature. For instance, the nonlinear dynamics of a slender CB with a lumped mass under primary parametric base excitation were investigated theoretically and experimentally in [1], where the governing nonlinear ODE was derived using Euler–Bernoulli beam theory. Nonlinear control strategies have also been developed to suppress fundamental-mode vibrations under external and parametric excitations [2]. In addition, vibration control frameworks incorporating viscous damping, aerodynamic drag, inertia effects, and geometric nonlinearities were proposed to enhance structural stability and improve bifurcation behavior [3]. Time-delayed position–velocity feedback control was shown to effectively suppress nonlinear oscillations and reduce transient and steady-state responses [4], while cubic velocity feedback controllers improve vibration mitigation near primary resonance conditions [5]. Furthermore, proportional–derivative and piezoelectric-based control strategies were successfully applied to composite CBs operating under subharmonic and superharmonic resonance conditions [6–8]. Despite these significant contributions, most studies are limited to simplified feedback structures, weakly nonlinear assumptions, or reduced-order analytical models. In particular, the combined effects of multi-level time-delayed nonlinear feedback, amplitude-dependent dynamics, and delay-induced stability transitions have not been sufficiently addressed within a unified analytical framework. This gap motivates the development of the present NPA for analyzing the nonlinear dynamics and stability characteristics of delayed CB systems.

Advances in smart structures, metamaterials, and nonlinear dynamical systems have

significantly broadened the scope of vibration analysis and control methodologies. For example, vibration localization in thin cylindrical shell structures was investigated using combined experimental, computational, and analytical approaches [9]. Piezoelectric metamaterial plates with tunable acoustic directivity were developed via shunted inductive circuits, enabling active reconfiguration of structural dynamic behavior through resonance tuning [10]. In addition, multiscale computational frameworks were employed to study the thermo-electro-mechanical response and stability characteristics of advanced piezoelectric metamaterials and shell-type structures [11]. Geometry-informed embedding techniques were also introduced to accurately capture localized discontinuities and nonlinear mechanical fields in complex structures [12]. Moreover, engineering applications involving nonlinear dynamic loading were further explored in [13]. Increasing attention has been directed toward nonlinear resonance enhancement and weak-signal detection in complex dynamical systems. In particular, weak multi-frequency fault signatures are often masked by strong background noise, which motivates advanced signal amplification techniques such as the fractional-order stochastic resonance (FSR) framework proposed in [14], where rescaling-frequency scanning imaging was used to enhance and visualize weak components. Although this study is formulated within an integer-order deterministic framework, these developments highlight the growing importance of delay effects, resonance phenomena, and memory-related mechanisms in nonlinear vibration analysis, instability prediction, and signal processing. Furthermore, MEMS-based nonlinear resonators continue to attract considerable attention due to their applications in sensing, signal processing, and precision engineering. The nonlinear dynamic response of a MEMS resonator subjected to abrupt mechanical shock and electrical excitation, including quintic nonlinear effects, was investigated in [15].

Oscillatory systems play a fundamental role in modeling dynamic phenomena across engineering, physics, biology, and transportation systems. In particular, nonlinear oscillations have attracted considerable attention due to their ability to exhibit complex behaviors such as bifurcations, hysteresis, jump phenomena, limit cycles, and chaotic transitions [16,17]. Accordingly, nonlinear oscillators are widely used as prototype models for studying amplitude-dependent and coupled dynamical systems arising in nonlinear science and engineering applications. Significant research has also been devoted to the effects of nonlinear restoring forces, damping mechanisms, and parametric excitation on the dynamic response of oscillatory systems [18,19]. Among these, Mathieu-type oscillators are of particular importance due to their wide applicability in structural dynamics, vibration control, and parametric resonance phenomena. These systems are governed by differential equations with periodic coefficients, where stability characteristics are typically described in terms of instability regions (Arnold tongues), which can be systematically analyzed using Floquet theory and related methods [20–23]. In addition, various perturbation-based and semi-analytical techniques have been developed to approximate solutions and predict resonance characteristics in Mathieu-type and related nonlinear systems.

Significant progress in nonlinear oscillation analysis was achieved through the development of HFF, which provides a systematic framework for estimating amplitude–frequency relationships in nonlinear oscillators [24]. Subsequent refinements extended its applicability to a wider class of nonlinear systems and improved the accuracy of frequency prediction procedures. However, the original and modified HFF formulations remain sensitive to the choice of evaluation points, for which no universal selection criterion has been established [25], which may affect the robustness of amplitude–frequency predictions. To address these limitations, several researchers introduced

weighted-residual approaches and modified trial functions for nonlinear oscillators, including systems with discontinuities and strong nonlinear restoring forces [26,27]. Further developments also focused on improving amplitude–period approximations by constructing equivalent linear representations of nonlinear systems, resulting in more stable analytical predictions and reduced divergence in nonlinear regimes [28–32]. Motivated by these limitations of classical and semi-analytical techniques, the NPA has emerged as an alternative framework for nonlinear dynamical analysis [33–36]. Unlike perturbation-based approaches, which depend on small parameters or asymptotic expansions, the NPA constructs an equivalent amplitude-dependent representation of nonlinear systems without requiring linearization or perturbation assumptions. This makes it particularly suitable for weak-to-moderate nonlinear oscillatory systems exhibiting amplitude-dependent behavior, time-delayed feedback effects, and stability transitions. Accordingly, we adopt the NPA framework to analyze the tri-level delayed nonlinear dynamics and stability characteristics of the controlled CB system. The key advantages of the NPA can be summarized as follows:

1. It provides a consistent equivalent representation of nonlinear dynamics while retaining the full set of original system parameters.
2. It offers a reliable and practically accurate approximation framework without claiming an exact closed-form solution.
3. It is readily extendable to a wide class of nonlinear dynamical systems with similar structures.
4. It demonstrates good agreement with numerical simulations, confirming its predictive capability and internal consistency.

The application of time-delayed nonlinear feedback control to externally excited CBs provides an effective strategy for vibration suppression; however, the combined influence of multi-level delays, nonlinear feedback gains, and amplitude-dependent inertia effects remains insufficiently understood, particularly in regimes where delay-induced phase shifts significantly affect stability behavior. This motivates the development of a unified analytical–numerical framework capable of capturing nonlinear response evolution, stability boundaries, and bifurcation characteristics of delayed structural systems. From an engineering perspective, such delayed feedback mechanisms are relevant to flexible structural and electromechanical systems, where phase-sensitive control plays a crucial role in vibration mitigation, resonance suppression, and stability enhancement.

To position the proposed approach within the literature, Table 1 compares the NPA with classical perturbation-based and semi-analytical techniques such as MTSM, the averaging method, and HBM. Unlike these conventional approaches, which rely on small parameters, averaging assumptions, or harmonic truncation, the NPA retains the full nonlinear governing equations and reformulates them into an amplitude-dependent equivalent representation, enabling direct stability characterization without perturbation expansion.

In this work, we focus on the application of an NPA-based analytical formulation to investigate nonlinear delayed vibration control in CB systems subjected to Mathieu-type excitation. The main contribution lies in developing an amplitude-dependent representation that facilitates the analysis of nonlinear resonance, stability behavior, and delay-induced effects within a unified analytical setting. The formulation retains the full nonlinear structure of the governing equations, including nonlinear stiffness, damping, inertia, and multi-level time-delayed feedback, while avoiding small-parameter assumptions and linearization procedures typically used in classical perturbation approaches. Within this context, the proposed approach enables direct characterization of stability transitions and nonlinear response evolution under combined parametric excitation and delayed control effects. The

major contributions of this work can be summarized as follows:

1. Development of an NPA-based analytical framework for a nonlinear delayed CB under Mathieu-type excitation.
2. Construction of an amplitude-dependent equivalent representation for nonlinear response and stability analysis without linearization or perturbation assumptions.
3. Integrated analytical–numerical validation using NDSolve simulations with quantitative error assessment, along with Floquet-based stability verification of periodic solutions.
4. Comprehensive characterization of nonlinear dynamics through transition curves, stability tongues, bifurcation diagrams, phase portraits, and Lyapunov exponent analysis.

Table 1. Comparative summary of the proposed NPA and conventional analytical approaches for nonlinear oscillatory systems.

Method	Main Assumption	Treatment of Nonlinearity/Forcing	Stability Treatment	Computational Complexity
MTSM	Small parameter	Taylor expansion and asymptotic reduction	Indirect via modulation equations	Moderate - High
Averaging Method	Slow variation	Averaged over one oscillation cycle	Approximate average stability	Low - Moderate
HBM	Periodic response	Harmonic truncation of response and forcing	Semi-direct via harmonic balance equations	Moderate
NPA	No perturbation parameter	Nonlinear terms incorporated through amplitude-dependent equivalent representation	Stability boundaries obtained from the equivalent formulation	Low

2. Construction of the problem

2.1. Governing nonlinear delayed model

The nonlinear delayed governing ODE describing the first-mode transverse vibration of a vertically mounted composite CB under Mathieu parametric excitation can be written as [37]:

$$\ddot{x} + 2\mu\omega_0\dot{x} + \omega_0^2 x + \alpha x^3 + \beta x\dot{x}^2 + \gamma x^2\ddot{x} = \eta f \Omega^2 x \cos\Omega t - H_C. \tag{1}$$

The governing equation includes several nonlinear and linear physical effects. The term αx^3 represents cubic nonlinear stiffness associated with Duffing-type hardening or softening behavior depending on the sign of α\alphaα. The term $\beta x\dot{x}^2$ introduces a quadratic velocity-dependent nonlinearity that contributes to nonlinear damping and inertial dissipation coupling. The term $\gamma x^2\ddot{x}$ accounts for nonlinear inertia, leading to amplitude-dependent effective mass and modified phase dynamics. The linear viscous damping is represented by $2\mu\omega_0\dot{x}$, which governs energy dissipation, while $\omega_0^2 x$ corresponds to the linear restoring stiffness controlling the natural frequency. Finally, the external excitation term $\eta f \Omega^2 x \cos\Omega t$ represents harmonic forcing that injects energy into the system and may induce resonance phenomena.

This formulation is dimensionless, with all variables and parameters normalized with respect to the characteristic modal properties of the CB. This facilitates stability analysis and enables systematic investigation of the relative influence of damping, excitation, nonlinear stiffness, and delayed feedback effects on the system dynamics.

The control input is formulated as a delayed nonlinear feedback force H_C, composed of displacement-, velocity-, and acceleration-dependent channels, each incorporating linear (p, q, g) and nonlinear (k, h, b) gain contributions along with distinct time delays ($\tau_1,\ \tau_2,\ \tau_3$). This multi-channel structure is designed to actively reshape the system dynamics through simultaneous stiffness modulation, damping redistribution, and inertial feedback regulation.

The feedback structure is expressed as:

$$H_C = px(t-\tau_1) + kx^3(t-\tau_1) + q\dot{x}(t-\tau_2) + h\dot{x}^3(t-\tau_2) + g\ddot{x}(t-\tau_3) + b\ddot{x}^3(t-\tau_3). \quad (2)$$

From a dynamical systems perspective, the interaction between nonlinear gains and time delays results in a nontrivial redistribution of energy between excitation and dissipation mechanisms, enabling either suppression or amplification of nonlinear oscillatory modes depending on parameter regimes. This introduces additional tunable nonlinearities that significantly influence stability boundaries, bifurcation behavior, and resonance characteristics. Table 2 provides a summary of the physical meanings and dynamical roles of the parameters in Eqs (1) and (2). The model incorporates linear and nonlinear stiffness, damping, inertia, and parametric excitation governing the nonlinear response and resonance behavior, while the feedback gains and time delays introduce active control effects and phase lag that critically affect stability and bifurcation characteristics.

A harmonic trial solution is assumed in the form [34–36]:

$$\tilde{x}(t) = B\cos\phi\, t. \quad (3)$$

This solution is adopted to describe the steady-state response of the system, where B denotes the initial amplitude, and ϕ is the total frequency of the controlled CB to be determined later. The ICs are specified as:

$$\tilde{x}(0) = B \text{and} \dot{\tilde{x}}(0) = 0. \quad (4)$$

These ICs define the initial state of the system and ensure a unique solution for the time-evolution problem. The tri-level delayed states are defined through time-shifted evaluations of the response, along with the trial solution as specified in Eq (3):

$$x(t-\tau_1) = x(t)\cos\phi\,\tau_1 - (\dot{x}(t)\sin\phi\,\tau_1)/\phi. \quad (5)$$

$$\dot{x}(t-\tau_2) = \dot{x}(t)\cos\phi\,\tau_2 + \phi x(t)\sin\phi\,\tau_2, \quad (6)$$

and

$$\ddot{x}(t-\tau_3) = -\phi^2 x(t)\cos\phi\,\tau_3 + \phi\dot{x}(t)\sin\phi\,\tau_3. \quad (7)$$

Time delays in displacement, velocity, and acceleration feedback significantly affect the system dynamics due to the phase lag introduced in the control loop. Specifically, displacement delay degrades positional accuracy; velocity delay reduces effective damping and may induce overshoot or sustained oscillations, while acceleration delay is particularly critical for high-frequency dynamics due to its sensitivity to rapid variations. Collectively, these delays introduce phase shifts that may alter stability characteristics and, if not properly tuned, can destabilize the system.

Table 2. Shows a summary of the dimensionless parameters used in Eqs (1) and (2).

Parameter	Physical meaning	Dynamical role
μ	Linear energy dissipation	Controls decay rate and linear damping effects
ω_0^2	Restoring elastic force	Governs natural frequency and baseline stability
f	External harmonic/parametric forcing intensity	Injects energy and may induce parametric resonance
Ω	Forcing frequency	Determines resonance regions and stability tongues
α	Duffing-type nonlinearity	Produces hardening/softening amplitude-dependent response
η	Velocity-dependent nonlinear dissipation	Modulates amplitude-dependent energy loss and saturation effects
γ	Amplitude-dependent inertia	Alters the effective mass and modifies dynamic phase behavior
p & k	Position-based control action	Enhances or suppresses displacement response and modifies stiffness
q & h	Velocity-based control action	Provides damping enhancement and vibration suppression
g & b	Acceleration-based control action	Influences inertial regulation and high-frequency response control
τ_1, τ_2, τ_3	Sensing/processing/actuation lags	Introduce phase shift, memory effects, and stability degradation or transition.

2.2. Physical and engineering relevance of the system

The proposed model applies to a wide class of flexible structural systems, including CBs, rotating machinery, and micro-scale resonators. Time-delayed feedback can be implemented experimentally using digital controllers and sensor-based feedback loops. In practice, additional sensing and processing delays may slightly modify the effective delay values, leading mainly to small shifts in stability boundaries.

Figure 1 illustrates the schematic of the considered smart CB, clamped at one end and free at the other, modeled as an Euler–Bernoulli beam. The structure is equipped with a surface-bonded MFC actuator and sensor. The actuator is near the fixed end, where bending strain is maximum, to generate controllable bending moments via the inverse piezoelectric effect, influencing the dominant modal coordinate in Eq (1). The MFC sensor converts strain into voltage signals proportional to displacement and its derivatives. These signals are processed through a feedback controller introducing time delays $\tau_1, \tau_2,$ and τ_3, which is consistent with the mathematical model. From an engineering perspective, the system applies to vibration suppression in aerospace structures, flexible robotic systems, rotating machinery, MEMS/NEMS resonators, and lightweight smart structures. Experimentally, it can be implemented using high-voltage amplifiers, data acquisition units, and digital signal processors to impose programmable delays, enabling validation of stability and nonlinear response predictions.

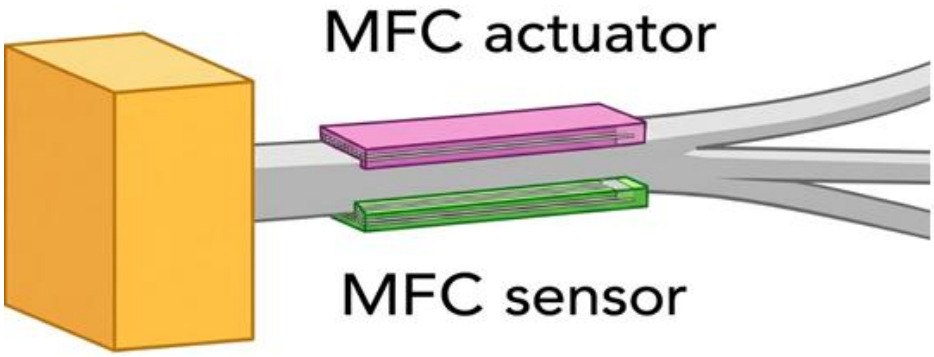


Figure1. A schematic of the considered CB structure.

2.3. Model consistency and limiting cases

To ensure the physical consistency and mathematical validity of the proposed formulation, several limiting cases are examined. Under suitable parameter reductions, the governing model recovers several well-established classical oscillatory systems reported in the literature:

1) Eliminating the delayed feedback contributions recovers the conventional parametrically excited CB model [1, 7].
2) When $f = 0, \beta = 0, \gamma = 0,$ and neglecting the feedback components with a negative stiffness factor, the model reduces to the damped softening Duffing oscillator [18].
3) In the absence of the factors $\mu = 0, f = 0, \beta = 0, \gamma = 0,$ and removing the delayed feedback terms, the model reduces to the Duffing-type oscillator $\ddot{x} + \omega_0^2 x + \alpha x^3 = 0$ [1, 38].
4) Removing the delayed feedback components and setting $\mu = 0, \eta = -1, \Omega = 1, \beta = 0, \gamma = 0,$ yields the classical linear parametrically excited Mathieu-type oscillator [22].
5) Neglecting damping, forcing, and delayed feedback terms $\mu = 0, p = k = q = h = g = b = 0,$ $\omega_0^2 = 1,$ and $f = 0$ yields the conservative Duffing oscillator $\ddot{x} + x + \alpha x^3 = 0$ [24, 28].
6) For$\eta = -1, \Omega = 2, \beta = 0, \gamma = 0,$ and the delayed feedback terms are removed, one obtains the standard damped Mathieu equation [38].

These limiting cases confirm that the proposed formulation provides a unified and physically consistent framework capable of reproducing classical oscillatory systems and advanced nonlinear controlled beam dynamics within a single generalized model.

The NPA is employed to study a forced cubic nonlinear CB subject to multi-level time-delayed position–velocity feedback. In contrast to traditional perturbation techniques that rely on small parameters, NPA reformulates the governing nonlinear delayed ODE into an amplitude-dependent equivalent representation while retaining the dominant nonlinear and delay-induced contributions, maintaining contributions from stiffness, damping, and delay influences. The method captures key dynamic features such as nonlinear resonance, amplitude–phase coupling, delay-induced stability shifts (including Hopf bifurcation), and hardening/softening performance due to detuning. It also assesses the role of feedback gains and delays. Analytical closed-form expressions for effective frequency and damping establish a direct connection between the model and physical response, supporting applications in vibration mitigation and stability control.

Accordingly, the controlled nonlinear Mathieu oscillator under multi-level delayed feedback can be reformulated as:

$$\ddot{x} + 2\mu\omega_0\dot{x} + (\omega_0^2 - \eta f\Omega^2 \cos\Omega t)x + \alpha x^3 + \beta x\dot{x}^2 + \gamma x^2\ddot{x} + px(t-\tau_1) + kx^3(t-\tau_1) + q\dot{x}(t-\tau_2) + h\dot{x}^3(t-\tau_2) + g\ddot{x}(t-\tau_3) + b\ddot{x}^3(t-\tau_3) = 0. \quad (8)$$

In accordance with the NPA procedure, Eq (1) is systematically reformulated as:

$$\ddot{x} + Q_1(x,\dot{x}) + Q_2(x) - \eta f\Omega^2(\cos\Omega t)x = 0, \quad (9)$$

where the nonlinear $Q_2(x)$ and damping $Q_1(x,\dot{x})$ functions represent secular terms and are fully incorporated into the equivalent linear system through the NPA procedure. These functions are expressed as:

$$Q_1(x,\dot{x}) = 2\mu\omega_0\dot{x} + R, \quad (10)$$

and

$$Q_2(x) = \omega_0^2 x + \alpha x^3 + \beta x\dot{x}^2 + \gamma x^2\ddot{x} + \Phi \quad (11)$$

where

$$R = (p/\phi)\dot{x}\sin\phi\tau_1 + q\dot{x}\cos\phi\tau_2 - (3k/\phi)x^2\dot{x}(\cos^2\phi\tau_1)(\sin\phi\tau_1) + (3k/\phi^2)x\dot{x}^2(\sin^2\phi\tau_1)(\cos\phi\tau_1) - (k/\phi^3)\dot{x}^3\sin^3\phi\tau + h\dot{x}^3\cos^3\phi\tau_2 + 3hx\dot{x}^2\phi(\cos^2\phi\tau_2)(\sin\phi\tau_2) + 3hx^2\dot{x}\phi^3(\cos\phi\tau_2)(\sin^2\phi\tau_2) + \phi g\dot{x}\sin\phi\tau_3 + 3b\phi^5x^2\dot{x}(\cos^2\phi\tau_3)(\sin\phi\tau_3) - 3b\phi^4x\dot{x}^2(\sin^2\phi\tau_3)(\cos\phi\tau_3) + b\phi^3\dot{x}^3\sin^3\phi\tau_3, \quad (12)$$

and

$$\Phi = px\cos\phi\tau_1 + qx\phi\sin\phi\tau_2 + kx^3\cos^3\phi\tau_1 + hx^3\phi^3 + \sin^3\phi\tau_2 - \Lambda^2 gx\cos\phi\tau_3 - b\phi^6x^3\cos^3\phi\tau_3. \quad (13)$$

A key aspect of the NPA framework is the identification of secular-like contributions and their separation into effects associated with nonlinear stiffness and nonlinear damping. In classical perturbation methods, secular terms arise due to resonance effects and may lead to unbounded growth in the perturbation solution over long time intervals, reflecting a limitation of asymptotic expansions rather than true physical instability [39–41]. In the NPA, these contributions are reformulated using an integration-based equivalent representation, which incorporates their effects into amplitude-dependent damping and frequency parameters. This leads to a bounded analytical approximation while retaining the dominant nonlinear behavior of the system. The effectiveness of this formulation has been reported in other studies for nonlinear oscillatory systems.

The NPA overcomes this limitation by identifying secular contributions directly at the governing ODE and transforming constant and quadratic nonlinear terms into analytically constructed odd functions through a structured integration-based procedure. This approach eliminates time-dependent growth while ensuring that nonlinear influences are consistently embedded within the equivalent damping and equivalent frequency parameters. The integration-based formulation underlying the NPA has been examined in other studies and provides a consistent framework for deriving explicit expressions of the equivalent dynamic factors. As a consequence, the reformulated system preserves

the intrinsic nonlinear characteristics of the original oscillator while maintaining bounded analytical conduct, particularly near primary resonance.

A trial (presumed) solution, which is subsequently anchored to the prescribed ICs of the equivalent linear system, can be given by:

$$\tilde{u}(t) = B\,cos\,\phi\,t. \tag{14}$$

With the ICs:

$$\tilde{u}(0) = B \text{ and } \dot{\tilde{u}}(0) = 0. \tag{15}$$

Substituting the presupposed trial solution into the original nonlinear ODE enables systematic identification of the equivalent damping and effective frequency, leading to the following equivalent linear formula:

$$\ddot{u} + \delta_{eqv}\dot{u} + \left(\varpi_{eqv}^2 - \eta f \Omega^2\,cos\,\Omega\,t\right)u = 0. \tag{16}$$

This relies on amplitude, enabling the linearized model to match the nonlinear response over a wide range.

2.4. Theoretical evaluation

The amplitude-dependent equivalent damping and frequency parameters are numerically evaluated using NDSolve via MS, following the analytical reformulation obtained through the NPA framework. These parameters are computed through definite integration over a complete oscillation cycle. This cycle-averaging procedure ensures that the effects of nonlinearities are consistently incorporated within the equivalent linear representation of the system. Integrating over a period $0 \to 2\pi/\phi$ enables the derived parameters to accurately reflect the net energy dissipation and effective stiffness of the original nonlinear oscillator (see [34–36] and [38–40]).

$$\delta_{eqv} = \int_0^{2\pi/\phi} \dot{\tilde{u}} Q_1(\tilde{u}, \dot{\tilde{u}})\,dt \Big/ \int_0^{2\pi/\phi} \dot{\tilde{u}}^2 dt, \tag{17}$$

and

$$\varpi_{eqv}^2 = \int_0^{2\pi/\phi} \tilde{u} Q_2(\tilde{u})\,dt \Big/ \int_0^{2\pi/\phi} \tilde{u}^2 dt. \tag{18}$$

For systematic stability and dynamic analysis, Eq (16) is rewritten in a normalized form. This yields a canonical structure where amplitude-dependent damping and frequency appear explicitly as constant factors, enabling clear analysis while retaining the system's key nonlinear features.

$$u(t) = \tilde{u}(t)\text{Exp}(-\delta_{eqv}t/2). \tag{19}$$

Herein, $\tilde{u}(t)$ represents the required time-periodic forcing function.
Substituting Eq (19) into Eq (16) yields the governing equation as follows:

$$\ddot{\tilde{u}} + (\Pi^2 - \eta f \Omega^2\,cos\,\Omega\,t)\tilde{u} = 0. \tag{20}$$

This takes the form of a standard Mathieu equation given by:

$$\Pi^2 = \varpi_{eqv}^2 - \frac{1}{4}\delta_{eqv}^2. \tag{21}$$

To facilitate analysis, the excitation frequency Ω is normalized. If T denotes the oscillation period, the normalized excitation frequency can be given by:

$$\Omega = \frac{\sigma}{T}. \tag{22}$$

At this point, the oscillation period is denoted by $T = 2\pi/\Lambda$, and Λ is the new overall system frequency. With this assumption, Eq (20) can be given as:

$$\ddot{\tilde{u}} + Z(\tilde{u}; t) = 0, \tag{23}$$

and

$$Z(\tilde{u}; t) = (\Pi^2 - \eta f \Omega^2 \cos \Omega t)\tilde{u}. \tag{24}$$

The goal is to rewrite Eq (20) in an equivalent linear formula with constant factors, resulting in:

$$\ddot{\tilde{u}} + \Lambda^2(\Pi)\tilde{u} = 0, \tag{25}$$

where the ICs are typically given as:

$$\tilde{u}(0) = A \text{ and } \dot{\tilde{u}}(0) = 0. \tag{26}$$

For this equivalent formulation, a trial solution consistent with Eq (25) and the ICs (26) can be proposed as:

$$\tilde{u} = A \cos \Lambda t. \tag{27}$$

Following the approach described in Eq (18), the new overall frequency can be computed as [34–39]:

$$\Lambda^2(\Pi) = \int_0^{2\pi/\Lambda} \tilde{u} Z(\tilde{u}; t)\, dt / \int_0^{2\pi/\Lambda} \tilde{u}^2 dt. \tag{28}$$

The numerical approximation of this frequency $\Lambda^2(\sigma)$ is then evaluated via the MS as:

$$\Lambda^2(\sigma) = \varpi_{eqv}^2 - \frac{1}{4}\delta_{eqv}^2 + \frac{\sigma f \eta (\sigma^2 - 2\pi^2)}{\pi^2(4\pi^2 - \sigma^2)} \Lambda^2 \sin 2\sigma. \tag{29}$$

The equivalent linear system obtained employing NPA offers a systematic way to identify stability boundaries of the controlled nonlinear oscillator, which can be formulated as follows:

$$\Lambda^2(\sigma) > 0 \tag{30}$$

and

$$\delta_{eqv} > 0, \tag{31}$$

where δ_{eqv} and Λ^2 are the amplitude-dependent equivalent damping and overall frequency factors, respectively.

The stability requirement is ascertained by the sign of Λ^2, the analogous linear ODE. Let $\Lambda^2 = \varsigma^2$ as shown in Eq (30). The preceding connection delineates the transition curve that distinguishes stable from unstable zones. The relationship $\Lambda^2 > \varsigma^2$ establishes a stable zone. This scenario

generates simple harmonic motion, and is situated above the transition curve. Conversely, as $\Lambda^2 < \varsigma^2$, one discovers the solutions of hypergeometric functions. This region is situated beneath the transition curve.

In this formulation, the nonlinear delay ODE is recast into a linear-like form where cubic stiffness, nonlinear inertia, and damping are incorporated into amplitude-dependent terms. This preserves key nonlinear influences while enabling analytical stability analysis. Findings are validated employing the MS, ensuring accurate agreement with the nonlinear model over a wide range of amplitudes and parameters. The framework efficiently captures steady-state and transient dynamics, stability limits, and nonlinear conduct while remaining physically consistent. The applicability of the present NPA formulation is subject to the following practical limitations:

i. The method is primarily intended for weak-to-moderately nonlinear oscillatory systems.
ii. The imposed initial conditions are assumed to remain unchanged throughout the equivalent reformulation procedure.
iii. Improved accuracy is generally achieved when the initial oscillation amplitude remains within the normalized range $0 < A \le 1$.

3. Validation and accuracy assessment of the proposed method

To verify the accuracy of the proposed analytical formulation, a systematic validation is performed through numerical comparison and error quantification. The validation includes:

(i) Time-domain comparison between the NPA solution and the numerical solution obtained via NDSolve via MS.

(ii) Quantitative error analysis to evaluate the deviation between the two solutions.

All simulations are carried out using adaptive time-stepping in NDSolve with sufficiently high accuracy and precision settings to ensure numerical convergence. The dimensionless parameters employed in the simulations are selected within physically realistic and numerically stable ranges commonly used in nonlinear delayed vibration-control studies. The chosen values ensure weak-to-moderate nonlinear oscillatory behavior that is consistent with the validity range of the proposed formulation. The adopted parameter set is listed below:

$$A = 0.5,\ \tau_1 = 0.08,\ \tau_2 = 0.05,\ \tau_3 = 0.04,\ f = 0.05, \gamma = 0.08, h = 0.05,\ \sigma = 0.3, \alpha = 0.03, b = 0.001,\ k = 0.01,$$

$$\omega_0 = 1.2,\ q = 0.05,\ p = 0.02,\ \beta = 0.01,\ \mu = 0.09,\ g = 0.05, \text{ and } \eta = 0.04.$$

Figure 2 presents the displacement–time response obtained from the analytical NPA formulation and the NS. The comparison is performed by plotting the displacement histories on the same graph to examine the agreement in amplitude and phase evolution. A close overlap is observed throughout the investigated interval $t \in [0,100]$, including the transient and steady-state regions. The obtained results indicate that the proposed NPA formulation provides a reliable approximation of the nonlinear dynamic response within the considered weak-to-moderate nonlinear parameter range.

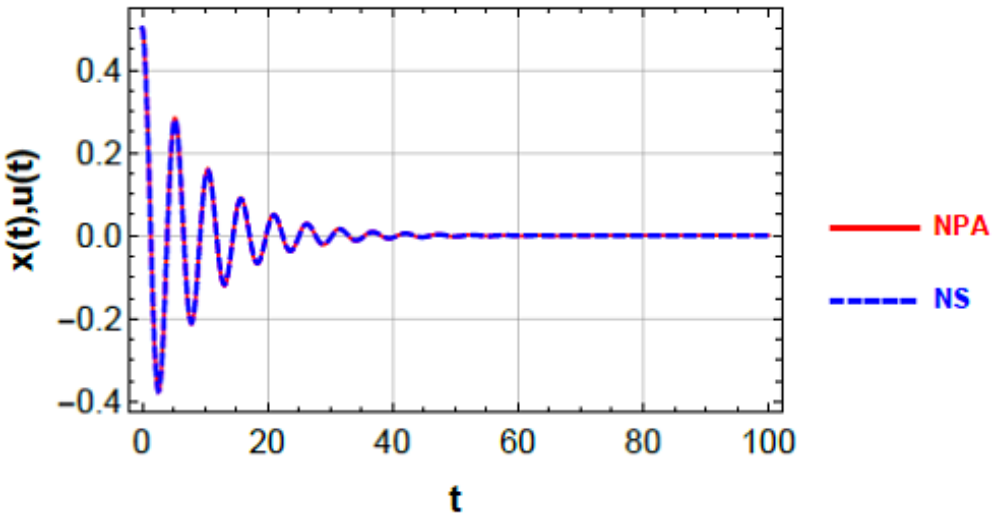


Figure 2. Shows a comparison between the NS of Eq (1) and the NPA solution of Eq (16).

To further quantify the difference between the NPA and NS results, the absolute error evolution is presented in Figure 3. The obtained error remains relatively small throughout the investigated simulation interval $t \in [0,100]$, indicating stable agreement between both solutions. During the initial stage of motion, the error increases slightly due to transient effects and the stronger contribution of nonlinear interactions. As the response gradually approaches steady-state motion, the error becomes nearly bounded within a narrow oscillatory range. No progressive growth or cumulative divergence is observed over the investigated time interval. These observations indicate that the proposed analytical NPA maintains consistent agreement with the numerical response for the considered weak-to-moderate nonlinear regime. The close correspondence between the displacement histories in Figure 2, together with the bounded error behavior in Figure 3, supports the applicability of the proposed NPA for the subsequent stability and dynamic analyses.

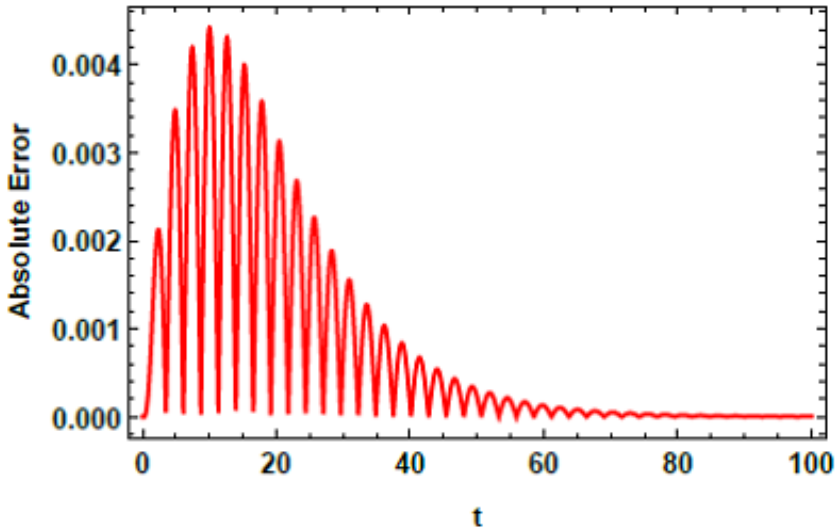


Figure 3. The time evolution of the absolute error between the NS and NPA solutions.

3.1. Error analysis and numerical accuracy based on tabulated results

Table 3 presents a comparative assessment between the NS and the proposed NPA solution over the time interval $t \in [0,100]$, together with the corresponding absolute error at selected time instants. The obtained results show close agreement between both solutions, with relatively small and bounded absolute errors throughout the considered interval. This behavior supports the consistency of the NPA within the investigated parameter range.

Table 3. Comparative evaluation between the NS obtained via NDSolve and the proposed NPA solution.

t	NS	NPA	Absolute error
0	0.500000	0.500000	0.000000
10	0.127241	0.131662	0.004422
20	0.013643	0.016355	0.002712
30	-0.006656	-0.005970	0.000686
40	-0.005102	-0.005231	0.000129
50	-0.002024	-0.002248	0.000224
60	-0.000532	-0.000660	0.000128
70	-0.000065	-0.000111	0.000047
80	0.000024	0.000013	0.000010
90	0.000020	0.000020	0.000000321
100	0.000008164	0.000009816	0.000001651

Table 4 summarizes the quantitative error metrics evaluated over the investigated time interval $t \in [0,100]$. The obtained results demonstrate strong consistency between the NS and NPA solutions, as reflected by the relatively small values of the Mean Absolute Error (MAE), Root Mean Square Error (RMSE), Normalized Root Mean Square Error (NRMSE), and Maximum Absolute Error (Max Error). In addition, the coefficient of determination (R^2=0.999709) indicates a very strong correlation between both responses. Therefore, the obtained error levels remain sufficiently small to support the applicability of the NPA within the considered weak-to-moderate nonlinear regime. The close agreement between the analytical and numerical responses further indicates that the proposed formulation adequately reproduces the dominant nonlinear dynamic behavior of the system without significant deviation over the investigated interval.

Table 4. Quantitative error analysis between the NS and NPA solutions over the interval $t \in [0,100]$.

Metric	Value	Interpretation
MAE	0.000730852	Indicates a very small average absolute deviation between the NS and NPA solutions.
RSME	0.0013193	Confirms good agreement over the interval.
Max Error	0.00442158	Shows that the worst-case deviation remains very limited.
NRMSE	0.00150906	Demonstrates that the normalized error is extremely small relative to the signal range.
R^2	0.999709	Reveals an almost perfect correlation between the NS and NPA solutions.

Table 5 shows that the Max Error and RMSE gradually increase with the oscillation amplitude. Nevertheless, the obtained error levels remain bounded and relatively small throughout the investigated amplitude range $0 < A \leq 1$, indicating that the proposed formulation maintains acceptable agreement with the NS for weak-to-moderate nonlinear oscillatory regimes. The observed increase in error is physically consistent with the stronger nonlinear interaction effects that arise at larger oscillation amplitudes, particularly near the upper limit of the investigated range.

Table 5. Variation of Max Error and RMSE with oscillation amplitude A over the interval $t \in [0,100]$.

A	Max Error	RMSE
0.2	0.00142703	0.000622637
0.4	0.00324806	0.00113324
0.6	0.00583108	0.00145519
0.8	0.00988874	0.00167219
1.0	0.0173786	0.00221602

The obtained results further indicate that the discrepancy between the analytical and numerical solutions does not exhibit cumulative growth over long-time integration.

3.2. Benchmarking and comparative assessment with analytical approaches

To evaluate the scope of the proposed formulation, this study is compared with CB vibration-control approaches reported in the literature [1,2,4,6–8]. In contrast to other studies, which rely on reduced-order or perturbation-based models and typically neglect explicit multi-delay effects, we introduce a tri-level delayed nonlinear feedback structure within a unified Mathieu-type CB framework. The proposed formulation further integrates stability maps, instability tongues, bifurcation analysis, and Floquet-based verification in a unified framework, offering a more comprehensive description of delay-induced nonlinear dynamics. Unlike earlier approaches that treat delays numerically or via linearization, this model embeds multiple delays directly into the governing nonlinear system, enabling clearer characterization of stability transitions and nonlinear response evolution. Accordingly, the NPA-based framework offers the following advantages:

- Incorporation of multi-delay feedback within a unified mathematical structure.
- Preservation of model consistency with improved analytical transparency and accuracy.
- Extension of classical CB vibration models to include higher-order nonlinear and delay effects.
- Capability to capture stability boundaries and bifurcation behavior without loss of nonlinear information due to linearization.

The major methodological differences are summarized in Table 6, highlighting contrasts in modeling assumptions, treatment of nonlinearity, and the resulting characterization of stability behavior.

Table 6. Comparative summary between this study and the related CB vibration-control study.

Study	System	Method	Delay Effect	Main Limitation/Scope
[1]	Parametrically excited CB with tip mass	Perturbation-based nonlinear analysis	Not included	No delayed feedback control
[2]	Single-mode active control of CB	MTSM	Not included	Single feedback channel
[4]	CB under parametric excitation	MTSM	Not included	Conventional feedback formulation
[6-8]	Flexible/composite beam vibration suppression	Perturbation / semi-analytical	Partially or numerically treated	Reduced-order or application-specific models
Present study	Mathieu-type nonlinear CB with tri-level delayed feedback	NPA + stability tongues + Floquet verification	Explicit multi-level delays	Weak-to-moderate nonlinear regime

4. Stability characteristics and dynamic response

The stability characteristics of the controlled CB are investigated through the equivalent linearized formulation derived via the proposed NPA framework. The transition curves obtained from the resulting characteristic relation define the boundaries separating stable and unstable oscillatory regions, thereby serving as direct indicators of the vibration suppression capability of the proposed tri-level delayed feedback strategy. In this framework, stable bounded motion occurs when the equivalent squared frequency remains positive, whereas instability emerges due to delay-induced phase effects and nonlinear energy-transfer mechanisms that lead to loss of synchronization between the structural response and the control action. From a control perspective, the region above the transition curve corresponds to effective vibration mitigation, where the combined position-, velocity-, and acceleration-feedback channels maintain bounded oscillatory motion through regulated energy dissipation. Conversely, the region below the transition curve represents reduced control effectiveness, where delay-induced phase mismatch promotes resonance amplification and instability. Hereafter, S and U denote the stable and unstable oscillatory regions, respectively. Figures 4–11 illustrate how the principal physical and control parameters influence the stability boundaries and vibration suppression performance of the system. Unlike conventional single-channel feedback strategies, the present tri-level delayed-feedback configuration enables simultaneous regulation of stiffness, damping, and inertial effects, thereby enhancing the flexibility and effectiveness of vibration control under nonlinear delayed dynamics. The dimensionless parameters employed in constructing these stability diagrams are listed as:

$$\tau_1 = 0.5,\ \tau_2 = 0.4,\ \tau_3 = 2.0,\ f = 0.5, \gamma = 0.2, h = 0.2,\ \sigma = 0.2, \alpha = 1.0, b = 0.2, k = 0.5,\ \omega_0 = 0.85, q = 1.2,$$
$$p = 0.5,\ \beta = 0.2,\ \mu = 0.5,\ g = 0.5, \text{ and } \eta = 0.5.$$

Figure 4 shows the influence of the linear viscous damping coefficient μ on the stability characteristics within the delayed-feedback configuration. The results show that increasing the

damping coefficient shifts the stability boundary toward a larger admissible oscillatory domain, indicating a stabilizing tendency under the considered control setting. Physically, viscous damping contributes to the reduction of vibration amplitudes and supports bounded-response behavior through energy dissipation mechanisms. However, the observed improvement in the stability region is configuration-dependent and results from the interaction between damping, nonlinear restoring forces, and delay-induced phase effects within the feedback loop. Accordingly, this shift reflects an enhanced vibration suppression performance of the controlled system under the delayed-feedback framework.

The variation of the cubic stiffness factor α on the stability characteristics is illustrated in Figure 5. For the set of delayed-feedback parameters, the stability diagram shows that increasing this parameter expands the stable oscillatory region, indicating a stabilizing tendency under the considered operating conditions. This behavior is associated with the amplitude-dependent nonlinear restoring force introduced by the cubic stiffness term, which modifies the effective oscillation frequency and redistributes the system energy over the oscillation cycle. Within the tri-level time-delayed feedback framework, the increased nonlinear stiffness influences the phase relationship between the structural response and the control action, which can improve synchronization under certain parameter ranges and thus enhance vibration suppression performance. Consequently, the stability boundary shifts toward higher admissible amplitudes, delaying the onset of instability. It should be emphasized that this behavior is configuration-dependent, as different delay settings or feedback gains may alter the phase interaction and lead to different stability trends.

Figure 6 shows the influence of the nonlinear coupling factor β on the stability characteristics. For the considered delayed-feedback configuration, the stability map shows that increasing this parameter reduces the stable oscillatory region, indicating a tendency toward reduced stability under the selected operating conditions. Physically, the nonlinear coupling term governs the interaction between displacement and velocity within the controlled restoring mechanism, resulting in stronger amplitude-dependent nonlinear effects as the coupling strength increases. Within the presence of time-delayed feedback, this enhanced nonlinearity increases the sensitivity of the phase relationship between the structural response and the control action, which may weaken the synchronization required for efficient vibration mitigation. As a result, earlier loss of stability and possible transition toward more complex oscillatory behavior may occur. It should be emphasized that this tendency is strictly configuration-dependent and is influenced by the selected delay parameters and feedback gains.

Figure 7 presents the influence of the nonlinear delayed position feedback gain k on the stability characteristics. For the chosen parameter range, the stability map shows that increasing this gain leads to a reduction in the stable oscillatory region, indicating a tendency toward reduced stability under the considered delayed-feedback configuration. This behavior is associated with the role of delayed position feedback as an amplitude-dependent corrective mechanism, where the gain magnitude and the time delay jointly determine its effectiveness. As the gain increases, the delay-induced phase shift between the structural displacement and the control force becomes more pronounced, which may weaken the synchronization between the system response and the feedback action. Under such conditions, the effectiveness of vibration mitigation may be reduced in certain amplitude ranges, leading to an earlier onset of instability. Consequently, the stability boundary shifts toward lower admissible operating regions, reflecting increased sensitivity of the system to delay-induced phase effects.

Figure 8 reflects the effect of the natural angular frequency ω_0 on the stability characteristics. For the considered parameter range, the stability map indicates that increasing the natural frequency

leads to a reduction in the stable oscillatory region, reflecting a tendency toward reduced stability under the delayed-feedback configuration. This behavior is related to the role of the natural frequency in governing the intrinsic stiffness–inertia balance and the fundamental oscillation rate of the structure. As the frequency increases, the system exhibits a faster dynamic response, which in turn alters the phase relationship between the structural motion and the time-delayed feedback forces. Since the effectiveness of delay-based control strongly depends on phase synchronization, higher natural frequency increases phase sensitivity and may result in partial loss of synchronization between the response and the control action. Consequently, the stability boundary shifts toward lower admissible operating regions, indicating an earlier onset of instability within the considered configuration.

Figure 9 presents the role of the linear velocity feedback gain q on the stability characteristics. For the delayed-feedback configuration, the stability map shows that increasing the velocity gain results in a gradual reduction of the stable oscillatory region, indicating a tendency toward reduced stability under the considered operating conditions. This behavior is attributed to the presence of a time delay within the tri-level control structure, where velocity feedback is intended to introduce damping but is applied with an inherent phase lag relative to the system's instantaneous velocity. As the gain increases, the effect of this delay becomes more pronounced, which may weaken the synchronization between the structural motion and the feedback action. The interaction between the velocity channel and the other feedback components further enhances phase mismatch, which affects the efficiency of energy regulation within the control loop. Consequently, the stability boundary shifts toward lower admissible operating regions, indicating an earlier onset of instability in this configuration.

Figure 10 demonstrates the role of the nonlinear inertial factor γ on the stability characteristics. For the configuration, the stability map indicates that increasing this parameter expands the stable oscillatory region, reflecting a stabilizing tendency under the considered delayed-feedback system. Physically, the nonlinear inertial term introduces an amplitude-dependent resistance to rapid motion, which moderates the acceleration response at higher vibration levels. This effect helps limit excessive dynamic amplification and influences the phase coordination between the structural response and the tri-level time-delayed feedback loops (position, velocity, and acceleration). As a result, the adverse effects associated with delay-induced phase lag are partially mitigated, leading to improved regulation of the system dynamics within the control loop.

Figure 11 presents the influence of the delayed displacement feedback factor τ_1 on the stability characteristics of the controlled CB. For the considered parameter configuration, the stability map indicates that increasing this factor enlarges the unstable oscillatory region, reflecting a tendency toward reduced stability within the delayed-feedback framework. In physical terms, the delayed displacement feedback introduces a control action based on past system states, which inherently produces a phase lag between the applied control force and the instantaneous structural response. As the feedback gain increases, the contribution of this delayed information becomes more significant in the overall control loop, thereby increasing the sensitivity of the system to phase-mismatch effects. Within the tri-level time-delayed feedback structure, this phase discrepancy may weaken the synchronization between the structural motion and the feedback action, which is essential for effective vibration regulation. As a result, the system exhibits a higher susceptibility to delay-induced dynamic transitions, leading to an earlier loss of bounded oscillatory behavior and a contraction of the stable operating domain. It is emphasized that this behavior is configuration-dependent and is governed by the selected delay parameters and feedback gains.

A comparative examination of Figures 4–11 reveals distinct parameter-dependent trends in the

stability behavior of the delayed nonlinear system, where the influence of each parameter is governed by its role in the nonlinear dynamics and its interaction with the time-delayed feedback structure. Overall, the results provide a sensitivity map that highlights the dominant factors governing stability modulation and the transition between bounded and unbounded responses. From a control-oriented perspective, the observed stability characteristics reflect the vibration suppression capability of the proposed tri-level feedback strategy. The coordinated action of position, velocity, and acceleration feedback contributes to regulating the system response; however, the presence of a time delay introduces phase-dependent effects that may either enhance or reduce control effectiveness depending on the operating regime. Consequently, the overall vibration mitigation performance is determined by the interplay between nonlinear structural dynamics, feedback gains, and delay-induced phase shifts, which collectively govern the synchronization between the structural response and the control action.

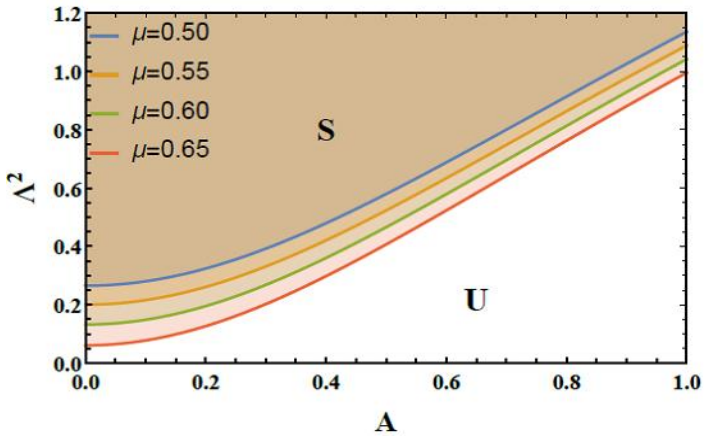


Figure 4. How μ affects the stability chart.

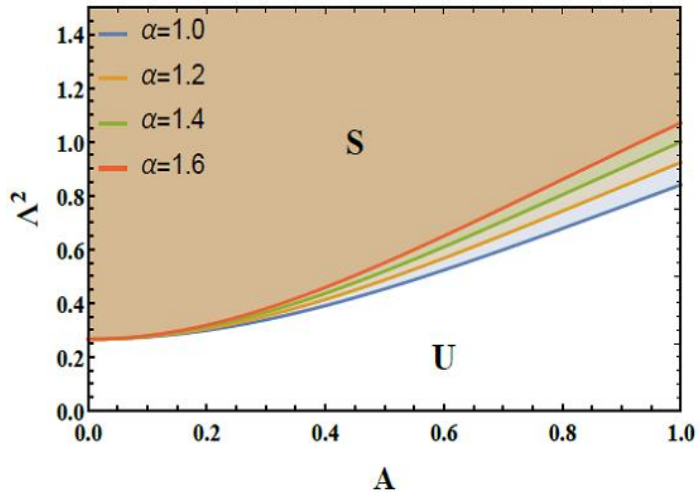


Figure 5. The role of α on the stability picture.

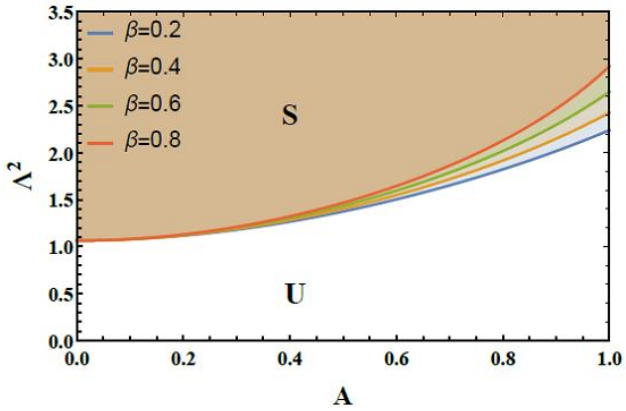


Figure 6. The role of β on the stability map.

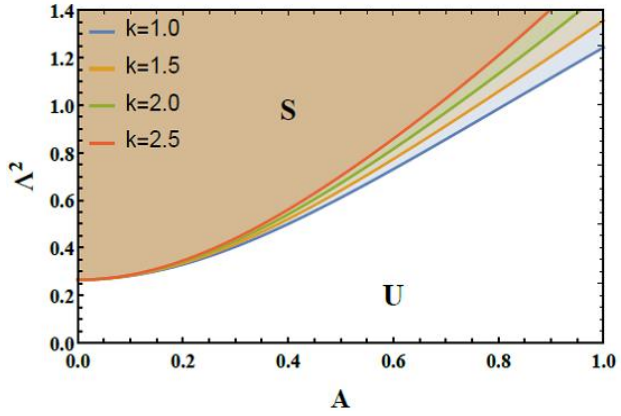


Figure 7. The role of k on the stability profile.

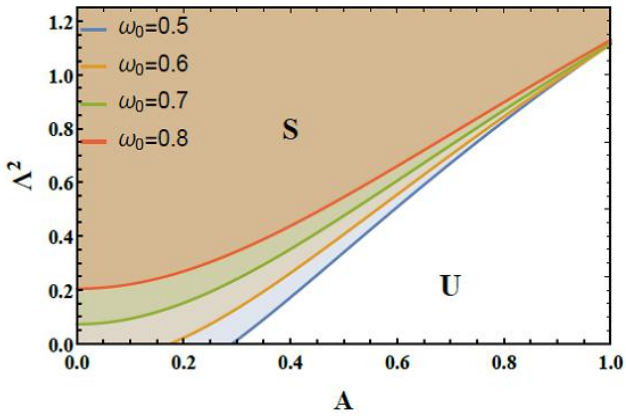


Figure 8. How ω_0 affects the stability scheme.

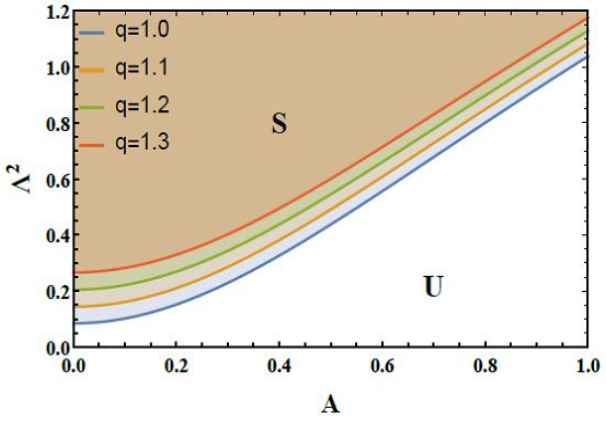


Figure 9. The conduct of q on the stability diagram.

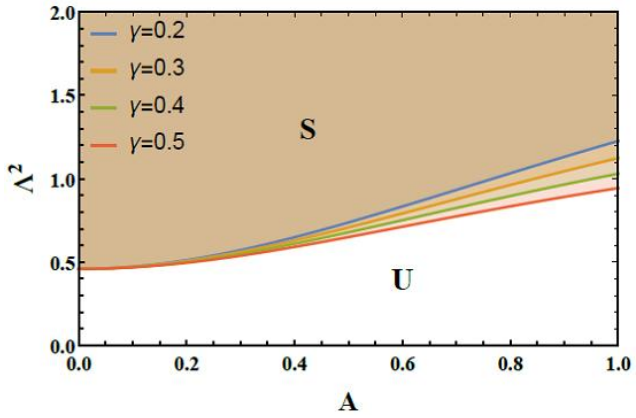


Figure 10. How γ affects the stability graph.

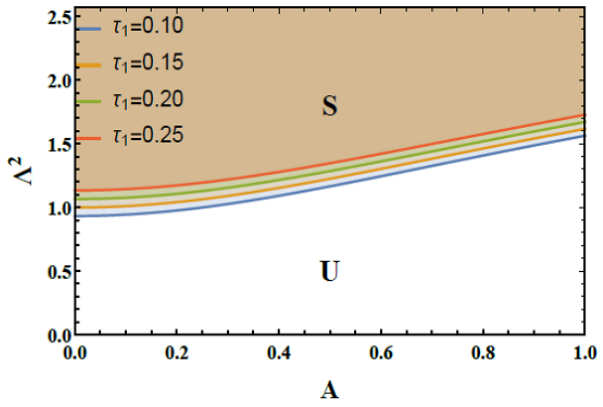


Figure 11. Exhibits the role of η on the stability map.

4.1. Stability evaluation via Floquet theory

The stability of the periodic solutions is further quantified using Floquet theory. The monodromy matrix is constructed by integrating the linearized variational equations over one excitation period, and the corresponding Floquet multipliers λ_i are obtained as its eigenvalues. The periodic solution is asymptotically stable when all multipliers remain inside the unit circle $|\lambda_i| < 1$, whereas instability occurs once at least one multiplier exits the unit circle. Accordingly, Figure 12 shows that the computed Floquet multipliers form a complex-conjugate pair located inside the unit circle, confirming the asymptotic stability of the corresponding periodic response for the considered parameter configuration. These results are consistent with the stability regions predicted from the transition curves and stability maps, thereby providing quantitative verification of the proposed NPA-based stability analysis. It is further noted that this analysis is performed for a representative parameter configuration, while all other system parameters are kept as defined in the previous sections, except $\mu = 0.005, \omega_0 = 1.0, f = 0.05, \sigma = 0.3,$ and $\eta = 0.01$.

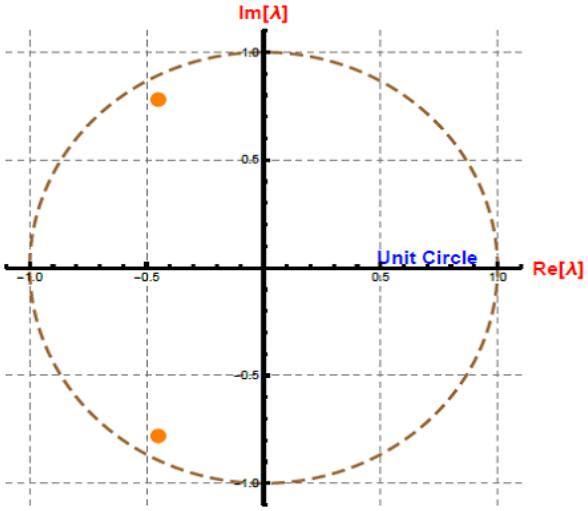


Figure 12. Floquet multipliers plotted on the complex plane.

4.2. Stability tongues

In what follows, the stability tongues are analyzed for a system having the following particulars:

$$A = 0.5,\ \tau_1 = 0.08,\ \tau_2 = 0.05,\ \tau_3 = 0.04,\ \gamma = 0.1, h = 0.03, \alpha = 0.15, b = 0.01,\ k = 0.02,$$

$$\omega_0 = 1.2,\ q = 0.08,\ p = 0.05,\ \beta = 0.08,\ \mu = 0.1,\ g = 0.08, \text{ and } \eta = 0.9.$$

Figure 13 presents the stability tongues of the delayed nonlinear system in the (Ω, f) plane. The obtained tongue-shaped regions identify the parameter combinations associated with transitions between stable, quasi-periodic, and chaotic responses. Stable bounded oscillations are observed for relatively low excitation amplitudes, whereas increasing the forcing amplitude progressively enlarges the instability regions. Near the tongue boundaries, the system exhibits quasi-periodic behavior, while the interior regions are characterized by chaotic dynamics, as confirmed by the corresponding phase

portraits, bifurcation diagrams, and Lyapunov exponent analysis presented in the subsequent sections. The gradual expansion of the instability tongues demonstrates the combined influence of nonlinearities and time-delayed feedback on the resonance structure and stability transitions of the system.

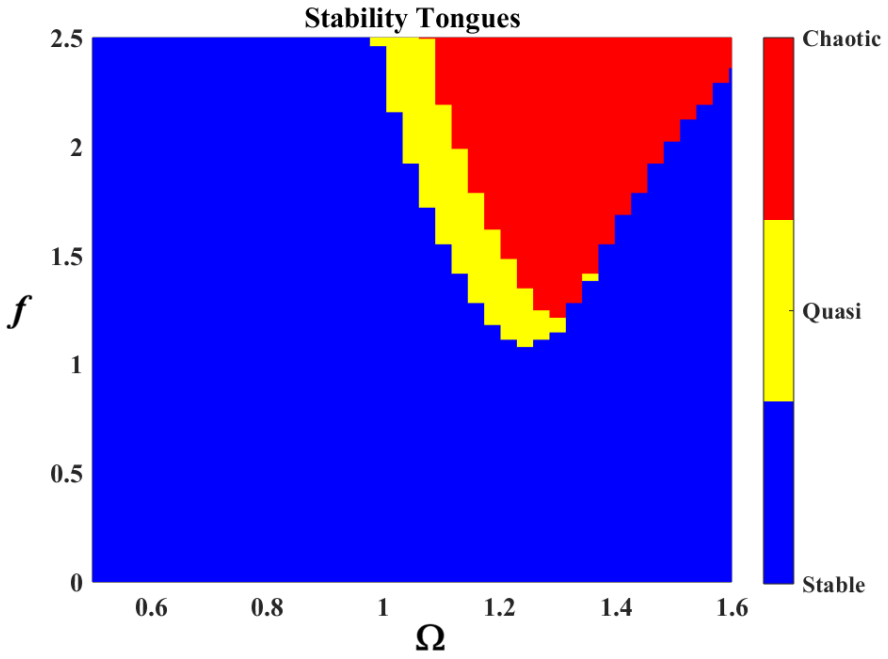


Figure 13. The stability tongues of the original time-delayed nonlinear ODE in the (Ω, f) plane, including stable, quasi-periodic, and chaotic regions.

Overall, the obtained stability characteristics are not inferred solely from qualitative observations, but are quantitatively supported through transition-curve analysis, stability tongues, Floquet-multiplier evaluation, bifurcation diagrams, and Lyapunov exponent calculations.

5. The system's chaotic response

The BDs, analyses of the LLEs, phase portraits, and PMs offer visual insights into the responses of dynamical systems to parameter variations. These analytical tools are complementary: BDs illustrate parameter-dependent response changes, and the LLEs assess stability and chaotic behavior. The inclusion of PMs further quantifies the characteristics of chaos and stability. Collectively, these tools establish a comprehensive framework for understanding complex dynamics, including transitions between stable and chaotic states [42].

The BD in Figure 14 illustrates the variation of the system response x with respect to the control parameter Ω. For low values of $0 \le \Omega \le 1.1$, the system exhibits a single steady-state solution, as indicated by the single horizontal branch. This reflects a stable periodic response. As Ω increases, the diagram shows the onset of bifurcation, where the single solution splits into multiple branches. This indicates a loss of stability of the original periodic motion and the emergence of more complex oscillatory behavior. With a further increase in $\Omega = 0.74$, the branches become increasingly dense and irregular, forming a broad band of scattered points. This dense structure is a classical signature of chaotic dynamics, where the system no longer follows a single periodic orbit but instead explores a

wide range of states in an aperiodic manner.

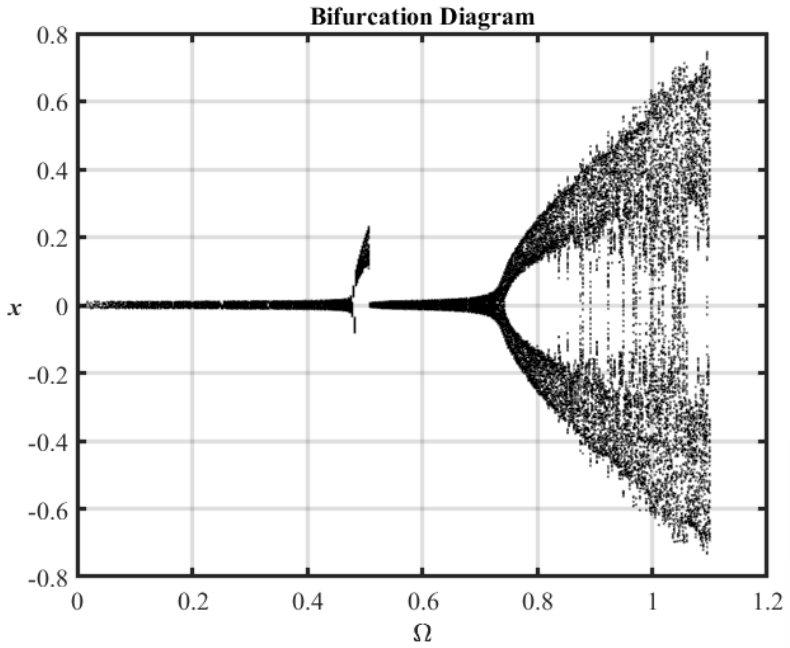


Figure 14. Shows BD vs. Ω.

Before arriving at the bifurcation-dominated transition area, the controlled CB changes from a simple periodic oscillation to a quasi-periodic motion within the interval $0.4 \le \Omega \le 0.6$ in Figure 14. The delayed-feedback-controlled system's innate nonlinear oscillation modes and the external parametric stimulation gradually interact to produce this quasi-periodic evolution. The excitation energy, delayed feedback loops, and nonlinear restoring force are somewhat synchronized in this range of excitation frequency, but the synchronization is no longer strong enough to maintain a single pure periodic orbit.

At smaller values of Ω, the beam physically functions in a stable periodic regime where a single principal frequency dominates the oscillation. The delayed controllers efficiently waste energy and preserve phase synchronization between the beam displacement and the control force in that area. However, the excitation frequency approaches internal nonlinear resonance conditions as Ω grows in the interval $[0.4,0.6]$. As a result, secondary oscillatory components start to interact with the dominant mode via delayed phase modulation and nonlinear coupling.

Two or more competing frequencies are produced in the response because of this interaction. After one oscillation interval, the resulting motion no longer repeats itself precisely because these frequencies are typically incommensurate. Rather, the quasi-periodic behavior seen in the bifurcation diagram is the result of the vibration's amplitude and phase continuously changing over time. Instead of collapsing onto a single closed periodic orbit, the system trajectory dynamically travels on a torus-like attractor in phase space.

The tri-level delayed feedback structure plays a significant role in this mechanism. Time-dependent phase delays are introduced into the restoring and dissipative forces by displacement, velocity, and acceleration feedback factors. These delays modify the timing of the feedback action enough to cause gradual amplitude modulation at moderate stimulation frequencies, but they do not

entirely destabilize the system. As a result, the oscillation is neither completely suppressed nor entirely amplified by the delayed forces. Rather, they provide long-term modulation envelopes that define quasi-periodicity by constantly redistributing energy between oscillatory modes.

Another crucial factor in creating this regime is the nonlinear stiffness term. The effective natural frequency becomes amplitude dependent due to the cubic nonlinearities in the restoring force. The instantaneous oscillation frequency varies slightly along with the oscillation amplitude during motion. External excitation and beam response experience nonlinear detuning because of this phenomenon. The system cycles between periods of partial synchronization and partial desynchronization instead of maintaining precise resonance locking. One of the major physical processes causing quasi-periodic evolution is this kind of nonlinear frequency modulation.

Energy exchange between dynamic components of the motion is facilitated simultaneously by the nonlinear inertial and coupling factors. There is no longer a consistent dissipation of the excitation energy delivered into the system over each cycle. Rather, energy oscillates between competing nonlinear modes, resulting in a gradual variation of the phase and amplitude of vibration. Instead of a single isolated limit cycle, this behavior manifests as nested or slightly deformed closed curves in the phase portrait. Accordingly, rather than discrete periodic points or entirely dispersed chaotic distributions, the PM would show ordered closed loops or closely spaced invariant curves.

Therefore, from the standpoint of bifurcation, the interval $0.4 \le \Omega \le 0.6$ can be described as a precursor transition zone that comes before the start of substantial instability. Nearby trajectories are constrained, and the LLE is around zero or slightly negative, indicating that the system has not reached a chaotic regime. However, due to delayed feedback modulation and nonlinear phase interactions, the periodic attractor has lost tight stability. This results in a confined but non-repeating oscillation that is quasi-periodic.

The equilibrium between energy injection and energy dissipation is another significant physical explanation. The delayed controllers effectively eliminate vibrational energy in the periodic domain, preserving steady oscillation. The control system and the beam dynamics become slightly coordinated during the quasi-periodic interval. Depending on the instantaneous phase relation, the delayed feedback can act constructively or dissipatively. Consequently, the beam undergoes alternating periods of amplification and attenuation. Thus, without creating total instability, this sporadic balancing creates modulation patterns in the response amplitude.

Thus, the quasi-periodic regime is a sign that a key nonlinear transition is about to occur in the system. The beam shows bounded motion under this dynamically sensitive operating condition, but it is more vulnerable to parameter perturbations and delayed phase effects. Within this range, slight variations in the excitation frequency, feedback gains, or delay values can cause the system to either go toward bifurcation cascades and chaos or back toward stable periodic oscillation.

The LLEs diagram in Figure 15 provides a quantitative measure of the system's sensitivity to ICs. For small values of Ω, the LLE remains negative, indicating that nearby trajectories converge, and the system is dynamically stable. As Ω increases, the exponent approaches zero, signaling a critical transition point where the system loses stability and quasi-periodic motion may arise. Beyond this region, the LLE becomes positive and remains predominantly above zero for a range of Ω. This behavior is a definitive indicator of chaos, confirming that trajectories diverge exponentially and the system exhibits sensitive dependence on ICs. The fluctuations observed in this region reflect the complex and irregular nature of chaotic dynamics.

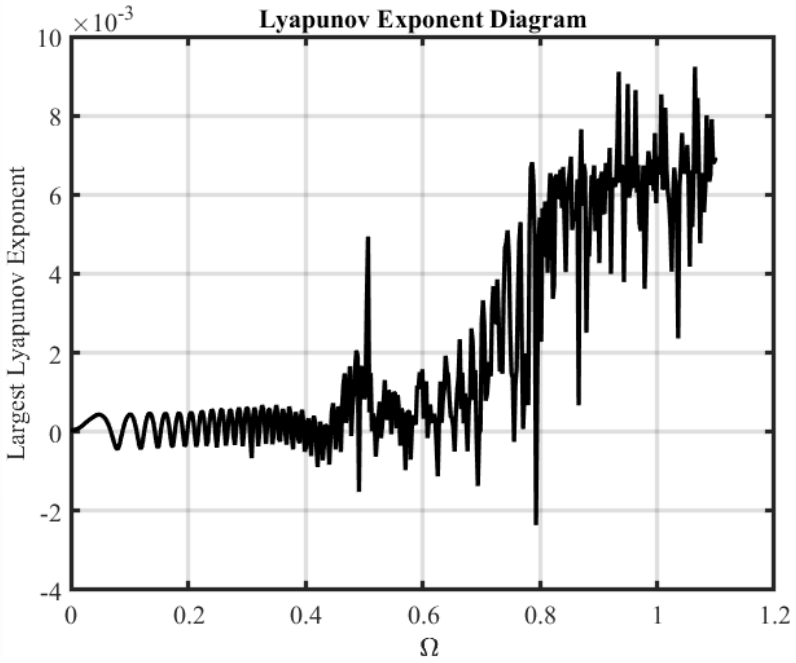


Figure 15. LLE diagram vs. Ω.

To determine the sensitivity of the nonlinear delayed CB system to beginning circumstances and to identify transitions from periodic motion to chaos, it is necessary to compute the LLE. In this work, the LLE is calculated numerically from the governing nonlinear delayed differential equation by tracking the exponential divergence of close solutions while integrating the system trajectories over long enough time intervals. To prevent numerical overflow during long-time integration, the numerical process relies on reconstructing the delayed oscillator's state-space dynamics and repeatedly normalizing perturbation vectors. This approach offers a thorough description of the controlled beam system's stability, quasi-periodicity, and chaotic behavior.

The governing nonlinear delayed equation is first rewritten into an analogous first-order dynamical system to begin the numerical computation. Instantaneous and delayed state variables are included in the phase space since the system possesses delayed displacement, acceleration, and velocity feedback components. Assume that the state vector is shown as

$$X(t) = [x(t), \dot{x}(t)]^T,$$

with delayed contributions assessed using the specified delay relations. Using NDSolve in the MS environment, a high-precision adaptive Runge–Kutta technique is used to numerically integrate the nonlinear system. Concurrently, a nearby disturbed trajectory

$$X'(t) = X(t) + \delta X(t),$$

is formed utilizing an initially small perturbation magnitude, usually selected between 10^{-8} and 10^{-10}. The two trajectories' instantaneous separation distance is then calculated as

$$d(t) = \|\delta X(t)\|.$$

This perturbation's average exponential growth rate is used to calculate the LLE in accordance with

$$\lambda = \lim_{t\to\infty} \frac{1}{t} ln \frac{d(t)}{d_0},$$

where the initial disturbance size is indicated by d_0. Chaotic motion is indicated by positive values of λ, stable periodic responses by negative values, and quasi-periodic or bifurcation-transition regimes by values around zero.

Through integration, the perturbation vector is regularly renormalized for numerical stability and accuracy. In the absence of renormalization, the perturbation may either expand excessively in chaotic regions or collapse near zero in stable parts, leading to numerical errors. The perturbation magnitude is reset to its initial value while maintaining its direction in phase space following each normalization interval Δt_r. The final LLE estimate is then calculated by averaging the cumulative logarithmic stretching factors across the integration duration. This process guarantees convergence and keeps finite-precision numerical mistakes from contaminating the exponent.

The nonlinear beam dynamics are strongly dependent on the excitation frequency, delay parameters, and feedback gains, according to the LLE's sensitivity study. The exponent becomes very sensitive to modest changes in parameters at the critical bifurcation period $\Omega \approx 0.7-0.8$. The coexistence of several competing attractors and the beginning of period-doubling bifurcations are reflected in the substantial changes in trajectory divergence rates caused by small changes in excitation frequency. The LLE varies around zero in this area, suggesting sporadic shifts between weak chaos and weak stability. This sensitivity shows that phase synchronization between the control forces and the structural response is significantly influenced by the nonlinear delayed feedback loops.

The LLE distribution and the size of the chaotic zones are strongly influenced by the delay parameters, τ_1, τ_2, and τ_3. The phase lag between the restoring force and the beam displacement is increased by increasing the displacement delay τ_1. This broadens the chaotic domain and typically changes the LLE toward positive values. The equivalent damping qualities are significantly changed by the velocity delay τ_2. While high delays degrade dissipative efficiency and speed up chaotic divergence, moderate delays may lower the LLE and improve stability. Similarly, high-frequency inertial interactions are controlled by the acceleration delay τ_3. While longer delays exacerbate irregular oscillations and increase sensitivity to beginning conditions, smaller values enhance dynamic robustness and decrease the exponent magnitude. As τ_3 rises, the chaotic attractor therefore expands and gets more intricate.

Strong sensitivity effects on the Lyapunov spectrum are also produced by the feedback gains. Stronger chaotic fluctuations and a faster transition to positive LLE values result from increasing the nonlinear position gain k, which enhances amplitude-dependent stiffness nonlinearities. When there are delays, a large velocity feedback gain q may lead the system to become unstable because the delayed dissipative force acts out of phase with the structural velocity. This increases chaotic regions and decreases effective damping. On the other hand, by enhancing energy redistribution within the oscillation cycle and moderating rapid acceleration growth, raising the nonlinear inertial coefficient γ typically decreases trajectory divergence and shifts the LLE toward negative values.

The transient removal approach is an essential component of accurate Lyapunov exponent computation. Rather than the intrinsic long-term attractor dynamics, the first part of the numerical response frequently incorporates transient oscillations that are substantially impacted by the chosen initial conditions. When these transients are included in the exponent computation, the stability characterization may be artificially distorted, and findings may be deceptive. As a result, there are two

phases to numerical integration. The system is integrated over a sufficiently long transient interval, t_{tr}, in the first stage. During this time, the trajectories converge toward the asymptotic attractor and the initial transient oscillations decay. The actual Lyapunov averaging process does not start until this transient removal interval is finished.

The damping level and the system's characteristic oscillation period are typically used to determine the transient duration. Because delayed feedback can induce intermittent oscillatory bursts and gradual amplitude modulation before the attractor is fully established, the transient interval for strongly nonlinear delayed oscillators must be long enough. Before evaluating LLE, several hundred stimulation periods are frequently disregarded in practice. Next, if the cumulative average stabilizes as the integration time grows, the exponent's convergence is confirmed. The transient interval or overall simulation period must be increased if the computed exponent keeps changing dramatically.

Because bifurcation points and quasi-periodic regimes show protracted intermittent dynamics and sluggish convergence toward attractors, the transient removal technique is very crucial in these areas. When competing attractors coexist at $\Omega \approx 0.7-0.8$, the trajectories may briefly oscillate between several phase-space structures before settling on the dominant attractor. By eliminating these fleeting intervals, the computed LLE is guaranteed to represent the actual asymptotic dynamics rather than ephemeral numerical distortions. Transient elimination also keeps divergence rates from being overestimated in chaotic regimes due to early and fast separation of trajectories unrelated to the stationary weird attractor.

In Figure 16 ($\Omega = 0.1$), the phase portrait shows a thick, annular-like region rather than a thin, smooth closed curve. The Poincaré section displays a cluster of scattered points rather than a single point or a small discrete set. The interpretation can be stated as follows:

The phase plot and the corresponding Poincaré section in Figure 16 show the presence of a contracted annular or torus-like trajectory rather than a standard single-limit cycle. Because it indicates the existence of quasi-periodic oscillation rather than just periodic motion, this distinction is physically significant. Under mild excitation conditions at $\Omega = 0.1$, the nonlinear delayed CB system generates several incommensurate frequencies that interact to form the annular structure.

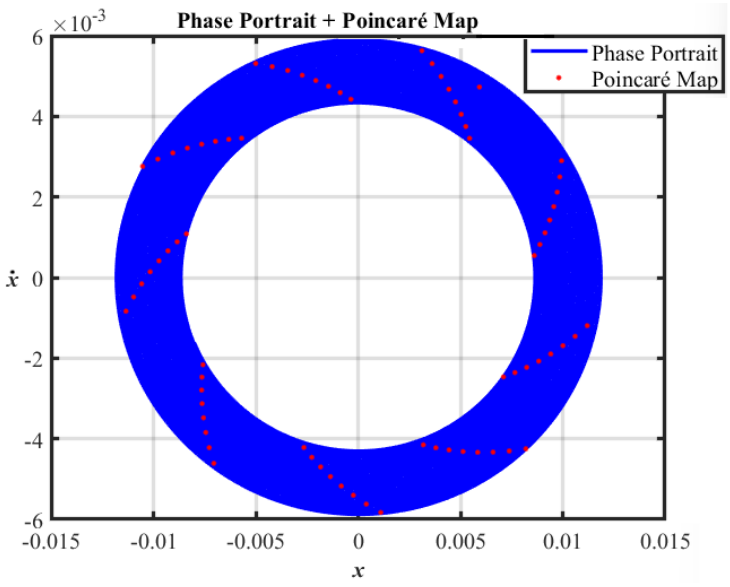


Figure 16. Phase portrait and PM diagrams at $\Omega = 0.1$.

One isolated closed orbit in phase space is what defines a valid limit cycle. In this scenario, regardless of the original conditions, every trajectory converges toward the same closed curve, and the system repeats its motion precisely after one oscillation period. Accordingly, there would only be one discrete point (or a finite number of isolated points for higher-period oscillations) in the Poincaré section of a limit cycle. Instead of collapsing onto a single closed orbit, the track in Figure 16 occupies a limited annular zone. In a similar vein, rather than a single isolated junction, the Poincaré section displays a distributed set of arranged points. These characteristics show that the oscillation has a sluggish phase and amplitude modulation, which is a characteristic of quasi-periodic dynamics.

The coexistence of two coupled oscillation frequencies within the beam response is linked to the underlying physical mechanism. The CB's main structural oscillation is the source of the first frequency, whereas parametric excitation and delayed feedback loops cause nonlinear modulation. The motion never fully closes after one cycle because these frequencies are not quite comparable. Rather, the trajectory fills an annular structure by continuously drifting around a restricted region in phase space.

Therefore, in the higher-dimensional delayed phase space, this annular attractor can be understood as a projection of an invariant torus. The effective phase space dimension is greater than that of a typical two-dimensional oscillator because the governing system includes terms for acceleration, velocity, and delayed displacement. The beam dynamics have additional internal modulation that naturally favors toroidal quasi-periodic motion instead of a simple periodic limit cycle because the delayed feedback introduces memory effects into the dynamics, which means that the motion depends not only on the instantaneous state but also on previous states evaluated at times $t - \tau_1, t - \tau_2,$ and $t - \tau_3$.

Nonlinear frequency detuning is another significant factor that causes the contracted annular trajectory. The effective natural frequency of the beam depends on the immediate oscillation amplitude due to the cubic nonlinear stiffness factor. The oscillation frequency fluctuates continually as the amplitude gradually increases over time because of delayed feedback interactions. The orbit is unable to precisely retrace the same route because of amplitude modulation and phase wandering. The trajectory thickens into a narrow band or annulus surrounding the mean oscillatory orbit rather than a thin closed curve.

This manner is further reinforced by the delayed acceleration and velocity feedback loops. Phase delays are introduced between the control action and the structural response by these feedback pressures. The delays provide continuous phase modulation at $\Omega = 0.1$, but they are not strong enough to cause chaos in the system. As a result, throughout subsequent oscillation cycles, the beam alternates continually between mild energy amplification and attenuation. The steady rotating drift around the annular attractor is caused by this gradual exchange of vibrational energy.

Energy-wise, the annular structure represents oscillatory energy that is bounded but continually modified. A pure limit cycle produces similar repeated motion because the energy balance between excitation and damping remains constant throughout each cycle. On the other hand, the quasi-periodic annular regime suggests that delayed phase synchronization and nonlinear interactions cause the energy balance to change slowly. As a result, the oscillation amplitude exhibits only slight variations while remaining within a bounded oscillatory range over the considered interval.

This interpretation is supported by the Poincaré section. The crossings provide a continuous or tightly packed closed set rather than discrete periodic points. A classical signature of quasi-periodic motion evolving on an invariant torus is such a distribution. While the lack of a single discrete point shows that the motion is not precisely periodic, the absence of irregular points distributed indicates that

the system has not reached a chaotic regime.

As a result, between fully chaotic behavior and stable periodic oscillation, the contracted annular trajectory seen in Figure 16 represents an intermediate nonlinear dynamical state. This reveals that the motion evolves on a quasi-periodic toroidal attractor rather than on a single periodic limit cycle, the system stays dynamically bounded and stable, multiple interacting frequencies coexist in the response, delayed feedback introduces slow phase modulation, and nonlinear stiffness causes amplitude-dependent frequency drift.

The bifurcation and Lyapunov studies in the manuscript, which show that the region before the chaotic transition is marked by quasi-periodic oscillatory evolution and a progressive loss of accurate periodic synchronization, are consistent with this explanation.

For higher values of $\Omega = 1.1$ in Figure 17, the phase portrait undergoes a significant transformation. The trajectories no longer form a single closed curve; instead, they spread over a broader region in the phase space, creating a complex structure characteristic of a strange attractor. The PM in this regime shows a scattered distribution of points with no apparent regularity or repetition. Unlike periodic motion, where points lie on discrete locations or smooth curves, the points here irregularly fill a region. This behavior confirms the presence of chaotic dynamics, where the system exhibits long-term unpredictability and sensitive dependence on ICs.

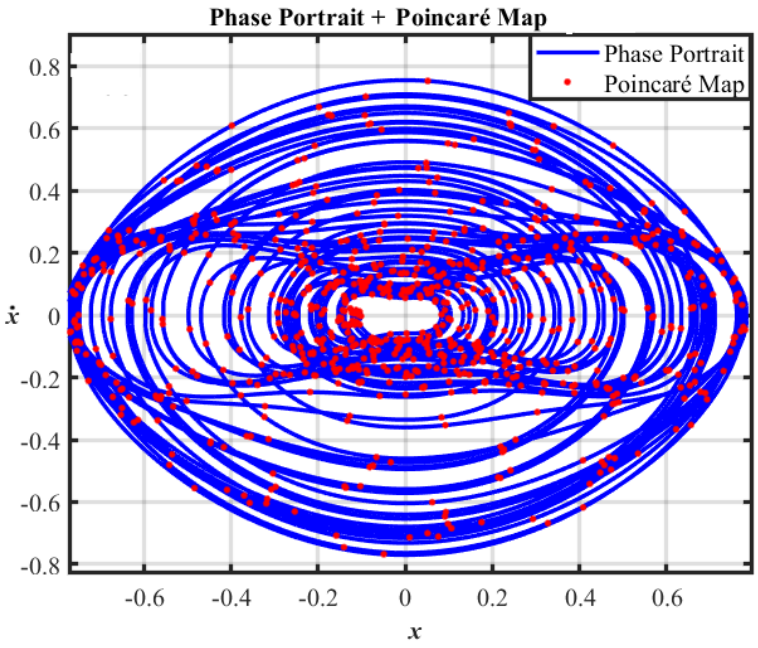


Figure 17. Phase portrait and PM diagrams at $\Omega = 1.1$.

Each graphical tool consistently supports the same conclusion: The system transitions from stable periodic motion to quasi-periodic behavior and to chaos as the parameter Ω increases. The agreement between the BD, LE, and geometric representations in phase space provides strong and reliable evidence of chaotic dynamics in the system.

Now, we are going to discuss the numerical error for the examined system when it transitions from a stable periodic motion into the quasi-periodic or chaotic regimes, as shown in the BD. As nonlinear delayed dynamical systems move from stable periodic motion to quasi-periodic and chaotic

regimes, the numerical error typically increases significantly. This increase is directly linked to the trajectories' increasing sensitivity to initial conditions, parameter perturbations, discretization mistakes, and cumulative round-off effects in the CB model. Strong evidence that the system gradually loses numerical robustness as Ω approaches the bifurcation and chaotic regions is provided by the bifurcation structures and positive LLE displayed in Figures 14–17.

The numerical error is very modest and under control within the stable periodic regime ($\Omega \leq 0.7$). Local truncation errors created during numerical integration are naturally eliminated by system dynamics in this region because all neighboring trajectories converge toward the same stable attractor. As a result, even if little round-off or discretization mistakes are produced at each integration step, they eventually decrease rather than increase. The negative LLE is a mathematical representation of this phenomenon. High numerical stability and great long-time agreement are confirmed by the reported absolute error between the analytical NPA approximation and the numerical solution, which is on the order of $10^{-5} - 10^{-8}$.

The numerical inaccuracy begins to significantly grow when the excitation frequency approaches the quasi-periodic transition interval ($\Omega \approx 0.7 - 0.8$). The Lyapunov exponent approaches zero in this region, suggesting that perturbations neither diverge instantly nor decay quickly. Instead, because of poor stability, mistakes linger for a long time and gradually compound. Particularly through the displacement, velocity, and acceleration delays, $\tau_1, \tau_2,$ and τ_3, the trajectories become more susceptible to phase changes brought about by the delayed feedback loops. Thus, during long simulations, small numerical errors result in discernible distortions in the phase trajectories and Poincaré sections. The coexistence of several neighbouring attractors intensifies this effect around bifurcation points because small numerical perturbations may lead the trajectory to flip between competing solution branches. As a result, instead of being entirely dissipative, the numerical error growth becomes algebraic or weakly exponential.

The chaotic regime ($\Omega \geq 0.8$) is where numerical inaccuracy increases the most. The LLE turns positive in this area, indicating that all minor perturbations, such as floating-point mistakes and numerical truncation, increase exponentially with time. Although both solutions are mathematically viable within the chaotic attractor, their paths diverge quickly if two numerical simulations begin with minusculely different initial circumstances or slightly different step sizes. Thus, even with precise short-term integration, long-term trajectory prediction is rendered impossible. This exponential divergence is not a result of the numerical approach failing, but rather an inherent feature of deterministic chaos.

6. Conclusions

In this study, we investigate vibration suppression in a flexible CB subjected to parametric excitation using a tri-level time-delayed nonlinear feedback control strategy incorporating position, velocity, and acceleration channels. The proposed control framework enhances the attenuation of structural vibrations compared to conventional instantaneous and single-channel linear feedback approaches. The analytical formulation is developed by employing the NPA, which transforms the original nonlinear delayed oscillator into an equivalent amplitude-dependent representation without relying on small-parameter expansions. The resulting model is validated through direct comparison with high-accuracy numerical simulations (NDSolve), demonstrating strong agreement in transient and steady-state responses. Delay-dependent stability maps reveal that time delays play a dual role:

They may enhance vibration suppression when properly tuned, but can also induce instability when phase synchronization between the structural response and feedback forces is lost. Furthermore, bifurcation analysis and Lyapunov exponent evaluations confirm the presence of rich nonlinear phenomena, including Hopf bifurcation, period-doubling, quasi-periodicity, and chaotic behavior, governed by the interaction between nonlinear restoring forces and delayed control actions. The major findings can be summarized as follows:

1) The proposed tri-level delayed feedback control significantly improves vibration attenuation of the CB compared to conventional linear or single-channel control strategies.
2) The combined position, velocity, and acceleration feedback structure provides enhanced flexibility for regulating nonlinear oscillations under parametric excitation.
3) The NPA formulation yields an effective amplitude-dependent representation of the nonlinear delayed system while maintaining consistency with numerical solutions.
4) The system exhibits complex dynamical behavior, including resonance shifts, multi-stability, and bifurcation scenarios governed by nonlinear and delay effects.
5) Stability (frequency–amplitude) maps provide a clear criterion for identifying transition boundaries between bounded and unstable responses.

Coupled CBs play a crucial role in engineering for applications such as vibration control, load sharing, and synchronized motion. They are utilized in structural engineering to enhance seismic and wind resistance in tall buildings and bridges, in mechanical engineering for stability in turbine blades and robotic arms, and in MEMS systems to enhance sensing accuracy in devices like biosensors and atomic force microscopes through dynamic interactions.

6.1. Practical guidance for control design

- Proper tuning of velocity gain, delay parameters, and natural frequency is essential to ensure stable operation and avoid delay-induced instability.
- Nonlinear inertial effects and appropriately scaled excitation can enhance robustness and enlarge the stable operating domain.
- The derived stability maps provide a practical design tool for selecting control parameters and predicting safe operating regions before implementation.

6.2. Future work

In future studies, researchers may extend this single-mode tri-level time-delayed NPA framework to multi-mode beam dynamics to capture higher-order modal interactions and delay-induced coupling effects. In addition, uncertainty quantification, parameter variability, and experimentally motivated delay models can be incorporated to assess robustness under realistic conditions. Researchers may also consider noise and estimation errors in velocity and acceleration reconstruction to enhance practical implementation fidelity.

Author contributions

Ahmad Almutlg: Resources, data curation; Galal M. Moatimid: Visualization, writing, review, and editing; T. S. Amer: Investigation, visualization, writing, review, and editing; Yasmeen M.

Mohamed: Methodology, investigation, formal analysis, data analysis and validation, software implementation, writing – original draft; writing – review and editing. All authors have read and agreed to the published version of the manuscript.

Use of Generative-AI tools declaration

The authors declare they have not used Artificial Intelligence (AI) tools in the creation of this article.

Acknowledgments

The Researchers would like to thank the Deanship of Graduate Studies and Scientific Research at Qassim University (www.qu.edu.sa) for financial support (QU-APC-2026).

Conflict of interest

The authors declare no conflicting interests.

References

1. L. D. Zavodney, A. H. Nayfeh, The non-linear response of a slender beam carrying a lumped mass to a principal parametric excitation: Theory and experiment, *Int. J. Nonlinear Mech.*, **24** (1989), 105–125. https://doi.org/10.1016/0020-7462(89)90003-6
2. A. F. El-Bassiouny, Single-mode control and chaos of cantilever beam under primary and principal parametric excitations, *Chaos Soliton. Fract.*, **30** (2006), 1098–1121. https://doi.org/10.1016/j.chaos.2005.09.015
3. A. Alanazy, A. T. EL-Sayed, F. T. El-Bahrawy, A non-perturbative methodology for a cantilever-beam dynamical system with bifurcation and negative derivative feedback controlling, *AIMS Math.*, **10** (2025), 17832–17867. https://doi.org/10.1016/j.apm.2010.06.020
4. S. S. Oueini, A. H. Nayfeh, Single-mode control of a cantilever beam under principal parametric excitation, *J. Sound Vib.*, **224** (1999), 33–47. https://doi.org/10.1006/jsvi.1998.2028
5. O. N. Ashour, A. H. Nayfeh, Adaptive control of flexible structures using a nonlinear vibration absorber, *Nonlinear Dyn.*, **28** (2002), 309–322. https://doi.org/10.1023/A:1015622630382
6. M. S. Rechdaoui, L. Azrar, Active control of secondary resonances piezoelectric sandwich beams, *Appl. Math. Comput.*, **216** (2010), 3283–3302. https://doi.org/10.1016/j.amc.2010.04.055
7. J. Warminski, M. Bochenski, W. Jarzyna, P. Fillipek, M. Augustyniak, Active suppression of nonlinear composite beam vibrations by selected control algorithms, *Commun. Nonlinear Sci. Numer. Simul.*, **16** (2011), 2237–2248. https://doi.org/10.1016/j.cnsns.2010.04.055
8. B. Pratiher, Vibration control of a transversely excited cantilever beam with tip mass, *Arch. Appl. Mech.*, **82** (2012), 31–42. https://doi.org/ 10.1007/s00419-011-0537-9
9. S. Kim, H. R. Moghaddasi, G. Franchini, F. Pellicano, M. Amabili, Symmetry breaking and vibrational mode localization in a circular cylindrical shell: Modeling and experiments, *Int. J. Mech. Sci.*, **322** (2026), 111681. https://doi.org/10.1016/j.ijmecsci.2026.111681

10. C. S. Schimidt, S. Janssen, L. P. R. Oliveirad, E. Deckers, C. Claeys, C. D. Junior, Sound directivity control in piezoelectric metamaterial plates via mode tailoring, *Int. J. Mech. Sci.*, **322** (2026), 111664. https://doi.org/10.1016/j.ijmecsci.2026.111664
11. Y. Zhang, S. Zhao, Y. Zhang, C. Lü, J. Yang, Multiscale thermo-electro-mechanical performance and stability of TPMS piezoelectric metamaterial shells, *Int. J. Mech. Sci.*, **322** (2026), 111665. https://doi.org/10.1016/j.ijmecsci.2026.111665
12. Z. Lai, L. Zhao, Q. Shao, Locally enhanced neural networks for discontinuities in solid mechanics, *Int. J. Mech. Sci.*, **322** (2026), 111660. https://doi.org/10.1016/j.ijmecsci.2026.111660
13. C. Liu, H. Wang, J. Zhang, S. Zhou, Y. Zheng, Engineering investigation of novel lightweight enhanced lateral effect shaped charge, *Int. J. Mech. Sci.*, **322** (2026), 111677. https://doi.org/10.1016/j.ijmecsci.2026.111677
14. Y. Gai, Z. Qiao, Y. Lu, R. Zhu, X. Zhang, Fractional-order stochastic resonance-based rescaling-frequency scanning images for early multi-frequency fault detection of machines, *Mech. Syst. Signal Process.*, **247** (2026), 113944. https://doi.org/10.1016/j.ymssp.2026.113944
15. M. E. Abdelraouf, A. Elsaid, K. Morino, W. K. Zahra, A. Kandil, Investigation of an electrically driven MEMS resonator under mechanical shock effect with quintic nonlinearity, *Mathematics*, **13** (2025), 3738. https://doi.org/10.3390/math13233738
16. A. H. Nayfeh, D. T. Mook, *Nonlinear oscillations*, Wiley, New York, 1979.
17. C. H. Miwadinou, A. V. Monwanou, L. A. Hinvi, A. A. Koukpemedji, C. Ainamon, J. B. C. Orou, Melnikov chaos in a modified Rayleigh Duffing oscillator with φ^6 potential, *Int. J. Bifurcat. Chaos*, **26** (2016), 1650085. https://doi.org/10.1142/S0218127416500851
18. K. Johannesen, The Duffing oscillator with damping for a softening potential, *Int. J. Appl. Comput. Math.*, **3** (2017), 3805–3816. https://doi.org/10.1007/s40819-017-0333-5
19. A. H. Salas, S. A. El-Tantawy, On approximate solutions to damped harmonic oscillator with higher-order nonlinearities and its application to plasma physics: semi-analytical solution and moving boundary method, *Eur. Phys. J. Plus*, **135** (2020), 833. https://doi.org/10.1140/epjp/s13360-020-00829-3
20. N. W. McLachlan, *Theory and applications of Mathieu functions*, Clarendon Press, Oxford, 1947.
21. L. N. Achala, Mathematical analysis and applications of Mathieu's equation revisited, *Int. J. Math. Appl.*, **9** (2021), 49–54.
22. I. Kovacic, R. Rand, S. M. Sah, Mathieu's equation and its generalizations: Overview of stability charts and their features, *Appl. Mech. Rev.*, **70** (2018), 020802. https://doi.org/10.1115/1.4039144
23. D. V. Ramani, W. L. Keith, R. H. Rand, Perturbation solution for secondary bifurcation in the quadratically-damped Mathieu equation, *Int. J. Nonlinear Mech.*, **39** (2004), 491–502. https://doi.org/10.1016/S0020-7462(02)00218-4
24. J. H. He, Comment on He's frequency formulation for nonlinear oscillators, *Eur. J. Phys.*, **29** (2008), L19–L22. https://doi.org/10.1088/0143-0807/29/4/L02
25. J. H. He, An approximate amplitude-frequency relationship for a nonlinear oscillator with discontinuity, *Nonlinear Sci. Lett. A*, **7** (2016), 77–85.
26. J. H. He, Amplitude-frequency relationship for conservative nonlinear oscillators with odd nonlinearities, *Int. J. Appl. Comput. Math.*, **3** (2017), 1557–1560. https://doi.org/10.1007/s40819-016-0160-0

27. Z. F. Ren, He's frequency-amplitude formulation for nonlinear oscillators, *Int. J. Mod. Phys. B*, **25** (2011), 2379–2382. https://doi.org/10.1142/S0217979211100370
28. Z. Ren, Theoretical basis of He's frequency-amplitude formulation for nonlinear oscillators, *Nonlinear Sci. Lett. A*, **9** (2018), 86–90.
29. A. Garcia, Amplitude-period formula for nonlinear oscillator, *Nonlinear Sci. Lett. A*, **8** (2017), 340–347.
30. R. S. Antola, Remarks on an approximate formula for the period of conservative oscillations in nonlinear second order ordinary differential equations, *Nonlinear Sci. Lett. A*, **8** (2017), 348–351.
31. D. Younesian, H. Askari, Z. Saadatnia, M. K. Yazdi, Frequency analysis of strongly nonlinear generalized Duffing oscillators using He's frequency–amplitude formulation and He's energy balance method, *Comput. Math. Appl.*, **59** (2010), 3222–3228. https://doi.org/10.1016/j.camwa.2010.03.013
32. Z. F. Ren, G. F. Hu, He's frequency–amplitude formulation with average residuals for nonlinear oscillators, *J. Low Freq. Noise Vib. Act. Control*, **38** (2019), 1050–1059. https://doi.org/10.1177/1461348418812327
33. R. K. Hussein, Y. M. Mohamed, A. T. El-Sayed, G. M. Moatimid, Vibration mitigation in a pitch–roll ship motion under multi-parametric excitations using proportional–derivative controllers, *Mathematics*, **14** (2026), 1100. https://doi.org/10.3390/math14071100
34. G. M. Moatimid, Y. M. Mohamed, M. K. Abohamer, Advanced non-perturbative and Galerkin scrutinizes of forced van der Pol–Duffing oscillator, *Int. J. Dyn. Control*, **14** (2026), 1–18. https://doi.org/10.1007/s40435-026-02021-4
35. G. M. Moatimid, Y. M. Mohamed, M. K. Abohamer, Advanced nonlinear dynamics and bifurcation structures in multi-coupled oscillators using a powerful non-perturbative framework, *Sci. Rep.*, **16** (2026), 12042. https://doi.org/10.1038/s41598-026-44027-0
36. G. M. Moatimid, Y. M. Mohamed, An innovative methodology in scrutinizing the nonlinear stability of two immiscible MHD viscoelastic liquids, *Math. Comput. Simul.*, **234** (2025), 472–496. https://doi.org/10.1016/j.matcom.2025.03.017
37. A. Mitura, J. Warminski, M. Bochenski, Optimal control methods for vertical and horizontal beam dynamics, *J. Phys. Conf. Ser.*, **382** (2012), 012041. https://doi.org/10.1088/1742-6596/382/1/012041
38. A. H. Nayfeh, B. Balachandran, Applied nonlinear dynamics: Analytical, computational, and experimental methods, Wiley, New York, 1995. https://doi.org/10.1002/9783527617548
39. Y. O. El-Dib, The masking technique for forced nonlinear oscillator stability behavior analysis using the non-perturbative approach, *J. Low Freq. Noise Vib. Act. Control*, **43** (2024), 1481–1497. https://doi.org/10.1177/14613484241253178
40. Y. O. El-Dib, Insights into transferal to fractal space modeling: Delayed forced Helmholtz–Duffing oscillator with the non-perturbative approach, *Commun. Theor. Phys.*, **77** (2024), 015002. https://doi.org/10.1088/1572-9494/ad7ceb
41. Y. O. El-Dib, Insightful and comprehensive formularization of frequency–amplitude formula for strong or singular nonlinear oscillators, *J. Low Freq. Noise Vib. Act. Control*, **42** (2023), 89–109. https://doi.org/10.1177/14613484221118177

42. T. A. Bahnasy, T. S. Amer, M. K. Abohamer, Stabilization of a nonlinear pitch-roll ship model via NVFBD control: Analytical and numerical investigations, *Ocean Eng.*, **354** (2026), 124944. https://doi.org/10.1016/j.oceaneng.2026.124944



AIMS Press

© 2026 the Author(s), licensee AIMS Press. This is an open access article distributed under the terms of the Creative Commons Attribution License (https://creativecommons.org/licenses/by/4.0)